DEFORMATION PROCESSES IN FORGING CERAMICS

Summary Report

February 1973

Prepared for

Office of Advanced Research and Technology
National Aeronautics and Space Administration
Headquarters
Washington, D.C.

Contract NASW-2187

Prepared by

R.M. Cannon
W.H. Rhodes

Approved by

T. Vasilos

T. Vasilos

AVCO CORPORATION
Systems Division
Lowell Industrial Park
Lowell, Massachusetts 01851

FOREWORD

This work was performed under the sponsorship of the NASA Headquarters, Office of Advanced Research and Technology, Research Division, with Mr. J. Gangler as Project Monitor under Contract NASW-2187.

The work was accomplished at the Avco Corporation, Systems Division, Lowell, Massachusetts in the Materials Sciences Department, managed by Dr. Thomas Vasilos. Mr. R.M. Cannon, Jr. directed the work with the assistance of Dr. W.H. Rhodes. The authors wish to acknowledge the assistance of Mr. B. MacAllister in Mechanical Testing and the Microscopy of Messrs. C.L. Houck and R.E. Gardner, and the X-ray diffraction analysis of Mr. P.L. Berneburg.

ABSTRACT

The program objective is to investigate the deformation processes involved in the forging of refractory ceramic oxides. A combination of mechanical testing and forging is being utilized to investigate both the flow and fracture processes involved.

Deformation studies of very fine grain Al_2O_3 revealed an apparent transition in behavior, characterized by a shift in the strain rate sensitivity from 0.5 at low stresses to near unity at higher stresses. The behavior is indicative of a shift in control between two dependent mechanisms, one of which is indicated to be cation limited diffusional creep with significant boundary enhancement. The possible contributions of slip, indicated by crystallographic texture, interface control of the diffusional creep and inhomogeneous boundary sliding are also discussed. Additional experiments indicated an independence of deformation behavior on MgO doping and retained hot pressing impurities, at least for ultrafine grained material, and also an independence of test atmosphere.

TABLE OF CONTENTS

I. INTRODUCTION 1

II. RESULTS 3

A. Stress-Strain Rate Tests 3
B. Crystallographic Texture 13
C. Hemisphere Forgings 18
D. High Temperature Fracture 27

III. DISCUSSION 31

IV. SUMMARY AND CONCLUSIONS 39

REFERENCES 40

APPENDIX

LIST OF FIGURES

Figure 1 Stress-Strain Rate Curves for the Sintered Material, LXII 5

Figure 2 Comparison of Flow Stress for As-Hot Pressed and Annealed Material 6

Figure 3 Stress-Strain Rate Curves for Fine Grained Al_2O_3 . . . 8

Figure 4 Flow Stress-Strain Rate Behavior of Hot Pressed Material, C126, Tested in Air 9

Figure 5 Stress-Strain Rate Curves of C126C Bars at 1400°C and 1490°C Showing the Effect of Reducing the Strain Rate 11

Figure 6 Corrected Stress-Strain Rate Curves for C126C and HP Materials 12

Figure 7 Strain Rate Versus 1/T Showing the Activation Energy for Deformation for the C126C and High Purity Material 14

Figure 8 Plot of the Strain Rate Dependence on Grain Size . . . 15

Figure 9 Ratio of Relative X-Ray Intensity for Compression Specimens Showing Basal Texture 17

Figure 10 Cracking of Deep Drawn Al_2O_3 Hemisphere 19

Figure 11 Premature Cracking in Hemisphere Run D1762 19

LIST OF FIGURES cont.

Figure 12 Fracture Surface of Crack Showing the Apparent Origin on the Surface Under the Punch 21

Figure 13 Microstructure of Outside Surface of Hemisphere D1442 22

Figure 14 Coarse Grained Patch from Piece of D1600 23

Figure 15 Cross-Section of Hemisphere D1442 Near the O.D. 24

Figure 16 Cross-Section of Hemisphere D1442 Near the Center . . .25

Figure 17 Cross-Section of Hemisphere D1442 Near the I.D. 26

Figure 18 Development of Crack from Growth and Connection of Triple Point and Grain Boundary Cavities 28

Figure 19 Compilation of Fracture Stress at Temperature for Polycrystalline Al_2O_3 29

Figure 20 Apparent Lattice Diffusivity Calculated from the Diffusional Creep Relation 34

Figure 21 Apparent Boundary Width-Diffusivity Product Calculated from the Diffusional Creep Relation 35

I. INTRODUCTION

The objective of this program has been to investigate the forgability of the refractory oxides. The approach taken emphasized an investigation of the relevant high temperature deformation and fracture behavior of these materials in order to provide information and understanding which can be applied directly to forging problems. In addition to mechanical properties studies, a few forgings were done to supplement the results.

The report for the first year included reviews of the reported work on the high temperature mechanical behavior of the oxides, including hot working efforts with these materials.[1] On the basis of this study, two systems were identified for primary investigation. These were fine grained alumina, doped to inhibit grain growth, and magnesia. For alumina, retention of a relatively fine grain size is important even at very high temperatures in order to obtain adequate ductility. For polycrystalline magnesia at temperatures of 2100°C or above, adequate ductility from slip processes was indicated as probable.

During the first year, extensive mechanical testing of fine grained alumina was performed to clarify the contributing deformation mechanisms at very fine grain sizes, to provide further data on flow stresses for use in forging, and to indicate the origins of cracking and cavitation at grain boundaries. In addition, a few forgings were done to correlate with the mechanical test results; these provided particularly valuable microstructural information.

Considerable evidence was found for increasing contributions of non-Newtonian deformation processes, including grain boundary sliding and dislocation motion, for grain sizes below 5 μ. Considerable capacity for deformation was also demonstrated although several causes of cracking were indicated. For most of the flexural tests and the forgings, the limiting cracks occurred at defective areas in the specimens which included coarse grained patches, pore nests and regions of impurity concentration. In addition, cavitation at grain boundaries also develops and presumably would be the limiting feature if the defective regions were eliminated in the specimens. The appearance and growth of cracks was shown to be faster at higher strain rates with the associated higher stresses.

During the past year on another program[2] some valuable comparative data were obtained on the deformation behavior of a higher purity alumina. This material, which had been specially made, had a grain size of 1.2 μ which made it almost identical to the C126C alumina tested during the first year of the present program except that it had a somewhat lower total impurity content and was not doped with 0.25% MgO as was that tested on this program. The results were extremely interesting in that the high purity material had nearly comparable flow stresses to the C126C data where comparable test conditions existed, but the high purity material exhibited generally higher values of rate sensitivity with m values between 0.77 and 0.93 in the range of 1228-1400°C compared to values of 0.65 to 0.71 for the C126C specimens. The second important difference was that higher flow stresses could be achieved before specimen fracture became a limiting feature.

During the present year, additional stress-strain rate tests were performed on the hot pressed Al_2O_3 + $\frac{1}{4}$% MgO material over an extended range of temperature and strain rate to compare with the high purity specimens. The combined results suggest a change in controlling deformation mechanism at low strain rates. In addition, tests were conducted in air on several different Al_2O_3 specimens to compare with previous[1] tests in argon in an attempt to resolve an apparent effect of either specimen purity or test atmosphere on flow stress. Finally, during this year some additional hemisphere forgings were attempted as well as some simple compression forgings to obtain highly strained material for microstructural evaluation.

The determination of atmosphere, impurity or dopant effects on the deformation behavior is of both theoretical and practical interest. Both altervalent impurities and atmosphere changes may be expected to change the defect concentrations in Al_2O_3, especially at the relatively low temperatures at which the fine grained material can be deformed. Such changes can be expected to effect both the cation and anion diffusivities which should directly affect the strain rate for several of the deformation mechanisms thought to be important for fine grained ceramics. In addition, differences in purity can also appreciably change the grain boundary chemistry by boundary segregation, and therefore may be important in grain boundary sliding. Finally, lattice impurities can influence dislocation motion by increasing the lattice drag on dislocation glide. As a result, a clearer understanding of the controlling deformation mechanism in fine grained Al_2O_3 may be indicated by determination of atmosphere and impurity or doping effects on the deformation kinetics and activation energy. A significant atmosphere effect on strain rate would be of practical importance in forging, where it is necessary to maintain sufficiently low stresses to prevent cavitation and cracking, but yet obtain sufficient strain rates to allow forging in reasonable times.

II. RESULTS

A. Stress-Strain Rate Tests

Three different batches of Al_2O_3 plus $\frac{1}{4}$% MgO were tested in flexure to determine the stress-strain rate behavior. A significant number of tests were done with an additional group of hot pressed, 1.2 μ* grain size, 99.8% dense specimens, which were taken from the same billet as the C126C specimens previously tested.[1] This material was made from a standard 99.9+% pure, 0.3 μ grade alumina powder with an addition of $\frac{1}{4}$% MgO for grain growth inhibition during pressing and testing. Data obtained on another program[2] for a higher purity Al_2O_3 will be presented for comparison. The high purity Al_2O_3 had been hot pressed from a special, high purity powder without any additives; it also had a 1.2 μ grain size and an essentially identical equiaxed microstructure. The high purity specimens had been found to have about 80 ppm total cation impurity and about 220 ppm anion and carbon impurity before testing; after testing the anion and carbon impurity was reduced to about 40 ppm and the cation impurity level was essentially unchanged.[2] Specific analyses are not available for the C126C material, but similar grades would be expected to have 2 to 3 times as high a cation impurity level, and perhaps higher anion and carbon impurity levels. Extensive tests also were conducted in argon over the temperature range 1192° - 1490°C; some additional tests were conducted in air for comparison. The high purity specimens had been tested in argon over a nearly comparable temperature range, but for tests at 1400°C and above there was significant grain growth which prevented comparative analysis of these data. Grain growth was less in the doped C126C specimens, although long tests at the higher temperatures were troubled by grain growth.

An additional series of tests in air were conducted on bars from a hot pressed billet, C42, of Al_2O_3 + $\frac{1}{4}$% MgO, which had an average grain size of about 2.7 μ. One set of bars was tested in the as-pressed condition. A second set of bars was annealed for 120 hours in air at 1300°C prior to testing. The annealing was conducted to reduce the gaseous species entrapped during hot pressing and to allow oxidation and escape of carbon retained from the hot pressing; the low temperature was chosen to minimize grain growth during annealing; the annealed specimens had a grain size about 10% greater than the as-pressed samples. The as-pressed samples were black; after annealing, the samples were significantly lighter although a dark shadow from the center remained. During annealing, the samples exhibited a small density loss of less than 0.1%, changing from slightly greater than 99.7% to slightly less than this value. The change in color is thought to result from oxidation and loss of carbon, but may also involve removal of other impurity or gaseous species. These specimens were tested at 1375° and 1450°C.

Finally an air test was conducted on the only remaining bar from the batch of sintered, Lucalox specimens from last year. This batch had a grain size of 15 μ and an average density of 99.2% of theoretical. This bar was tested at 1661°C.

All of the testing was done in four point flexure. Although separate furnaces were used for the argon and air tests, uniform procedures were used

---

*The grain sizes were all measured by the linear intercept method and reported as $G = 3/2\ \bar{L}$. Grain sizes were generally measured on as-tested bars; except where noted, they were little different from the as-pressed grain sizes.

as much as possible so that only the atmosphere would be changed. Both furnaces were calibrated to ensure comparable temperature measurements. The test machine is a constant cross-head drive machine with a variable speed drive. Incremental strain rate tests were performed by maintaining a constant deflection rate until a steady-state load was achieved and then increasing the rate to the next desired level and again waiting for steady-state. The load is continuously recorded versus time. The deflection is measured with a probe which activates a LVDT and is also continuously recorded. The probe system is used to measure inner knife edge deflection, D, which can be converted directly to outer fiber strain by the relation:

$$\epsilon = \frac{4hD}{\ell^2} \qquad (1)$$

where h is the specimen thickness, and ℓ the inner gauge length.

For the C126C tests, considerable effort was expended to achieve the lowest possible strain rates from the test machine. The argon system utilized a three probe deflection measurement system; this system seemed to be more accurate at the low rates, where total strains were small, than the single probe system used in the air furnace.

The outer fiber stress for each condition is calculated from the load curves using the relation:

$$\sigma = \frac{2M}{bh^2}\ (2 + n_b + m_b) \qquad (2)$$

where $n_b = \left(\frac{\partial M}{\partial \varphi}\right) \dot{\varphi}$ and $m_b = \left(\frac{\partial M}{\partial \varphi}\right) \varphi$, where M is the applied moment, b and h are the specimen breadth and depth, and φ is the included angle of bending. For these tests, steady-state conditions were achieved for which n_b was essentially zero.

The results of the air test on the 15 μ sintered bar are shown in Figure 1. This curve includes the results of the previous[1] argon tests for comparison. Although there is a small difference between the air and the argon results, the difference is very much less than the factor of four to five which was indicated to be possible by comparison of last year's results[1] with some earlier tests conducted in air.[3]

The C42 specimens were tested to determine whether carbonaceous impurities or other gaseous impurities would have a measurable effect on the deformation behavior. The test results are shown in Figure 2. Very little difference in behavior could be seen between the two groups; the slightly larger grain size of the annealed specimens would be sufficient to explain the slight indication of higher flow stress for this material. Because of the coarser grain size of this material, it had to be tested above 1300°C; as a result, the as-pressed materials became somewhat lighter during the tests (in which the sample is at temperature for two to three hours typically). At these low temperatures, some fine cracking and porosity generation occurred on the tensile surfaces and caused this side of the bar

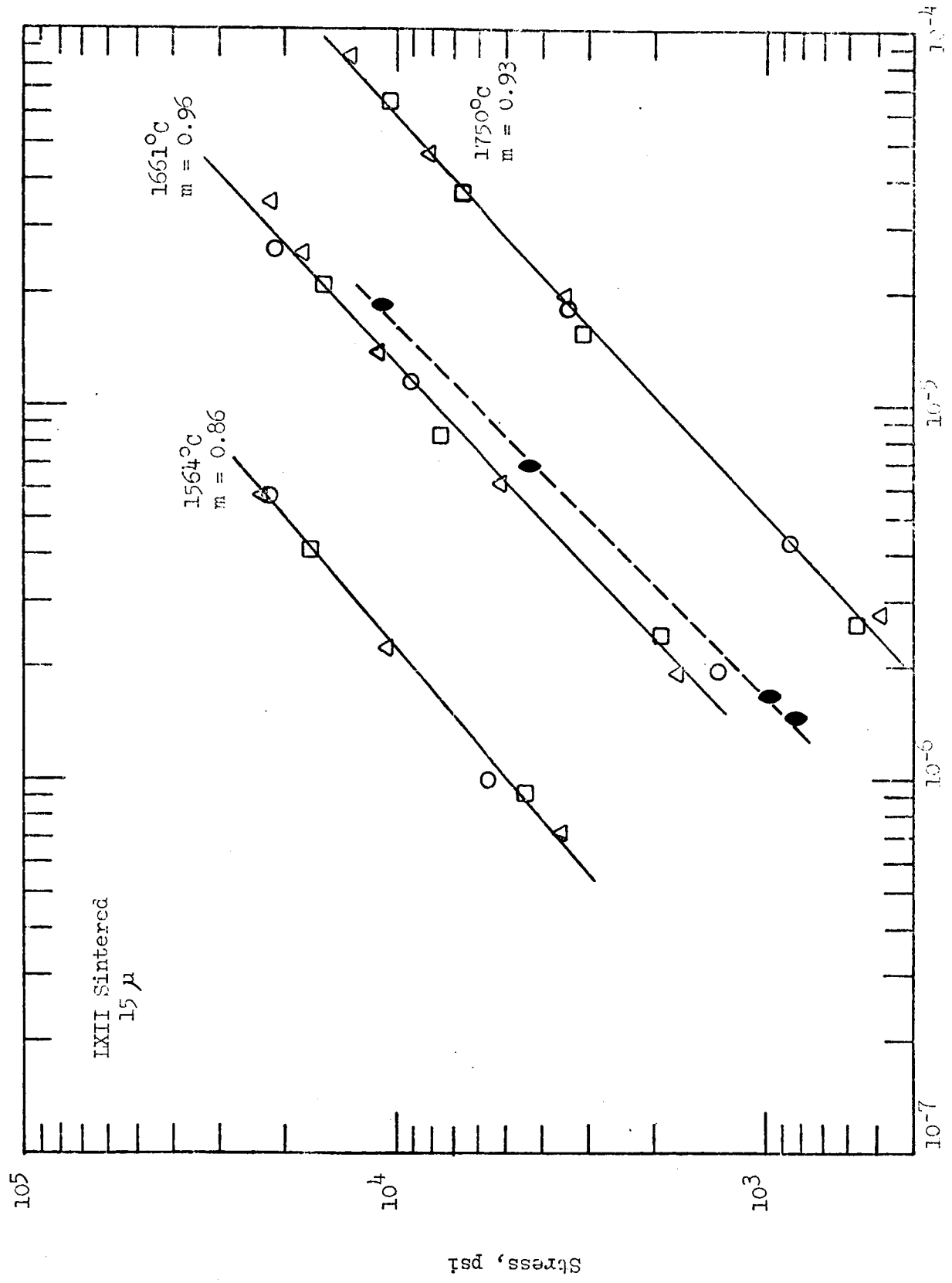

Figure 1. Stress-Strain Rate Curves for the Sintered Material, LXII, Comparing an Air Test (filled symbols) with Previous Argon Test Results.

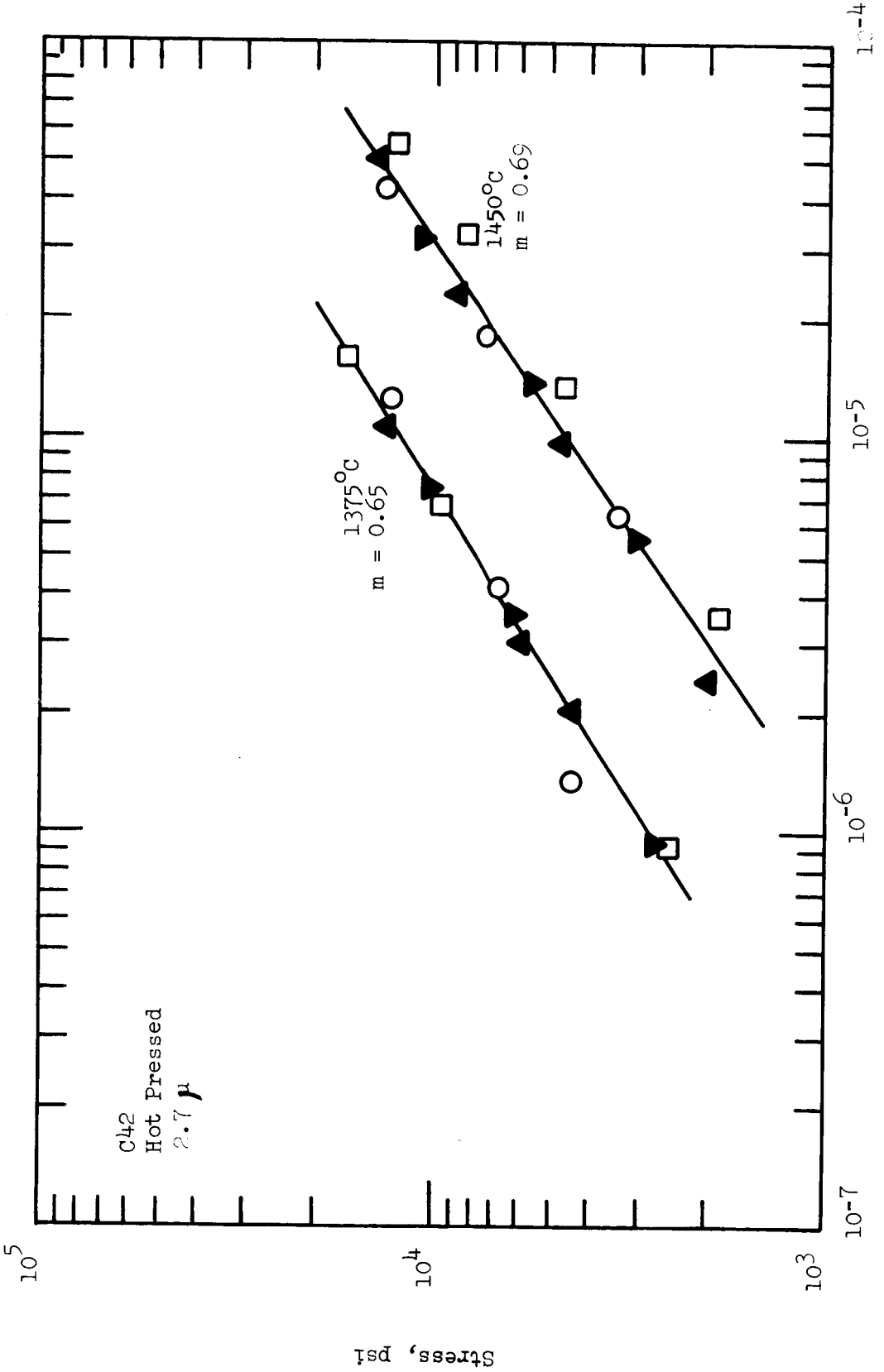

Figure 2. Comparison of Flow Stress for As-Hot Pressed and Annealed Material. The Filled Symbols are for Annealed Material.

to show a greater effect of annealing than the compressive side. Even though some annealing effects occurred, it is surprising that no differences in the two groups were apparent, especially in the initial test points for the as-pressed material. This suggests that if an effect of gases or carbon contamination exists, it is either very difficult to eliminate or else that the significant changes occur very quickly on heating in air even though color changes are slower to become apparent. After testing, it was observed that the annealed specimens exhibited somewhat more cracking and porosity generation during testing; this was surprising considering the small density change during annealing.

The results for the C126C tests in argon are plotted in Figure 3. This plot includes the data previously reported[1] plus the recent tests. The stresses for this plot have been calculated using the elastic approximation:

$$\sigma = \frac{6M}{bh^2} \qquad (3)$$

Also shown on the plot are the lines for the high purity tests at temperatures of 1228°, 1258°, 1288°, and 1337°C. A similar plot is shown in Figure 4 for the C126C tests in air.

These curves show an increase in strain rate sensitivity at the highest stresses or rates for each temperature, suggesting a transition in the rate controlling mechanism. The shift brings the C126C data into substantial agreement with the high purity data in the high range where comparable data exist. The authors were unaware of similar behavior in any ceramic systems although similar results had been reported in the superplastic literature[4,5,6]; in some of these cases, m values as low as 0.2 are observed at the lowest rates, and the maximum rate sensitivities observed before dislocation creep becomes dominant may be only as high as 0.5 to 0.8. Recently a similar observation has also been reported in Bi_2O_3 near the transformation temperature.[7]

There are two possible causes of systematic error which could contribute to this apparent shift in behavior. The points at the highest stresses are taken on bars with increasing strain and so have the greatest uncertainty in the bending moment because of horizontal load components at the load supports. As discussed in the Appendix, an analytic correction is possible, but the correction is very sensitive to the coefficient of friction between the knife edges and specimen. If the friction is negligible, the bending moment at large specimen curvatures would be even larger than that plotted here using the simple vertical load formula; however, if the coefficient of friction is high, the apparent stresses at large curvatures are too high. Arbitrary selection of a value of the coefficient of friction is not warranted and so no correction for this effect was made. However, comparison of these data with other test series and comparison of rate sensitivities of individual bars tested with different initial strain rates suggests that the increase in rate sensitivity is real, although some of the scatter in the data may be caused by specimen curvature effects. If a correction is made, assuming a sufficiently high coefficient of friction to straighten the stress-strain rate line,

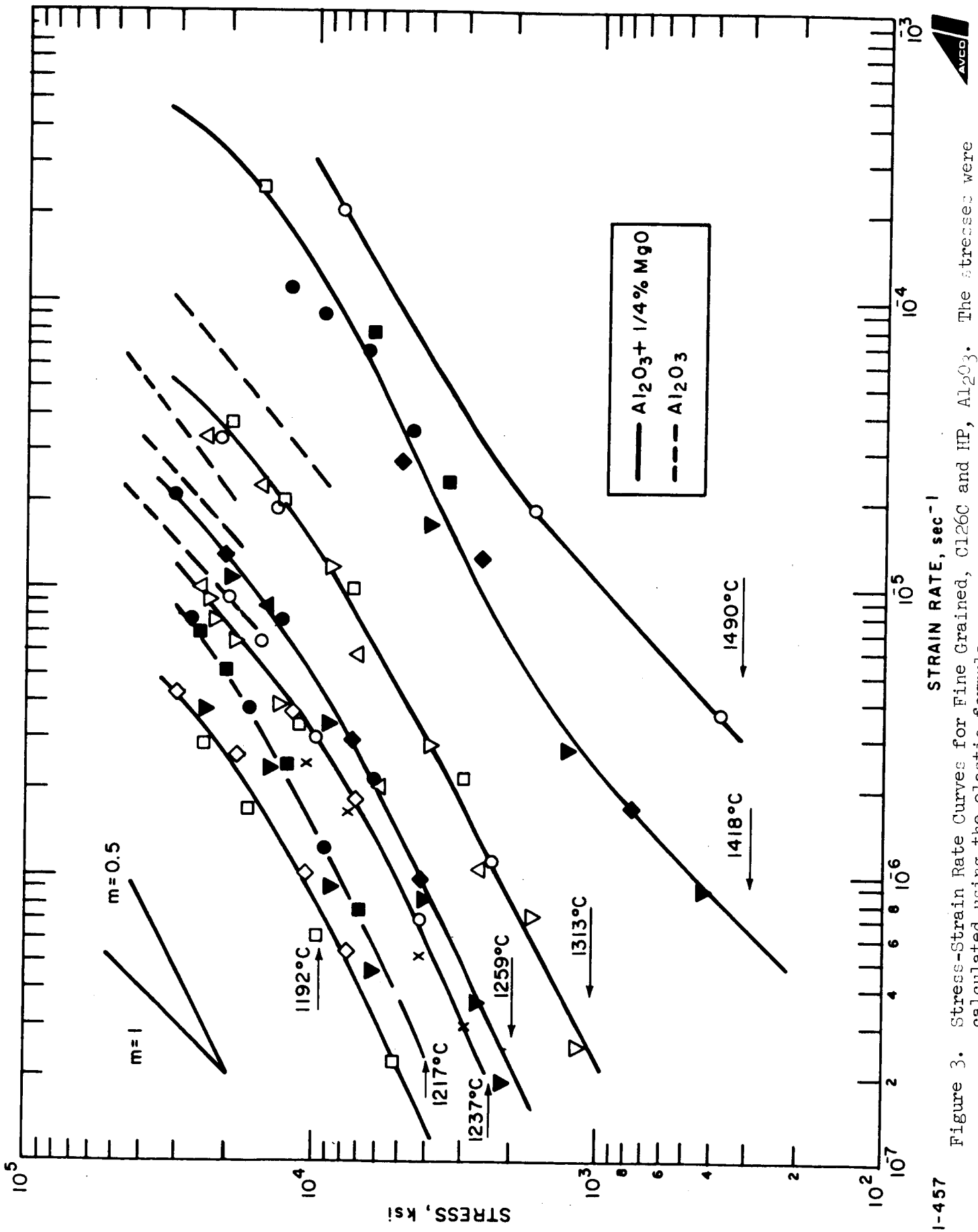

Figure 3. Stress-Strain Rate Curves for Fine Grained, C126C and HP, Al_2O_3. The stresses were calculated using the elastic formula.

71-457

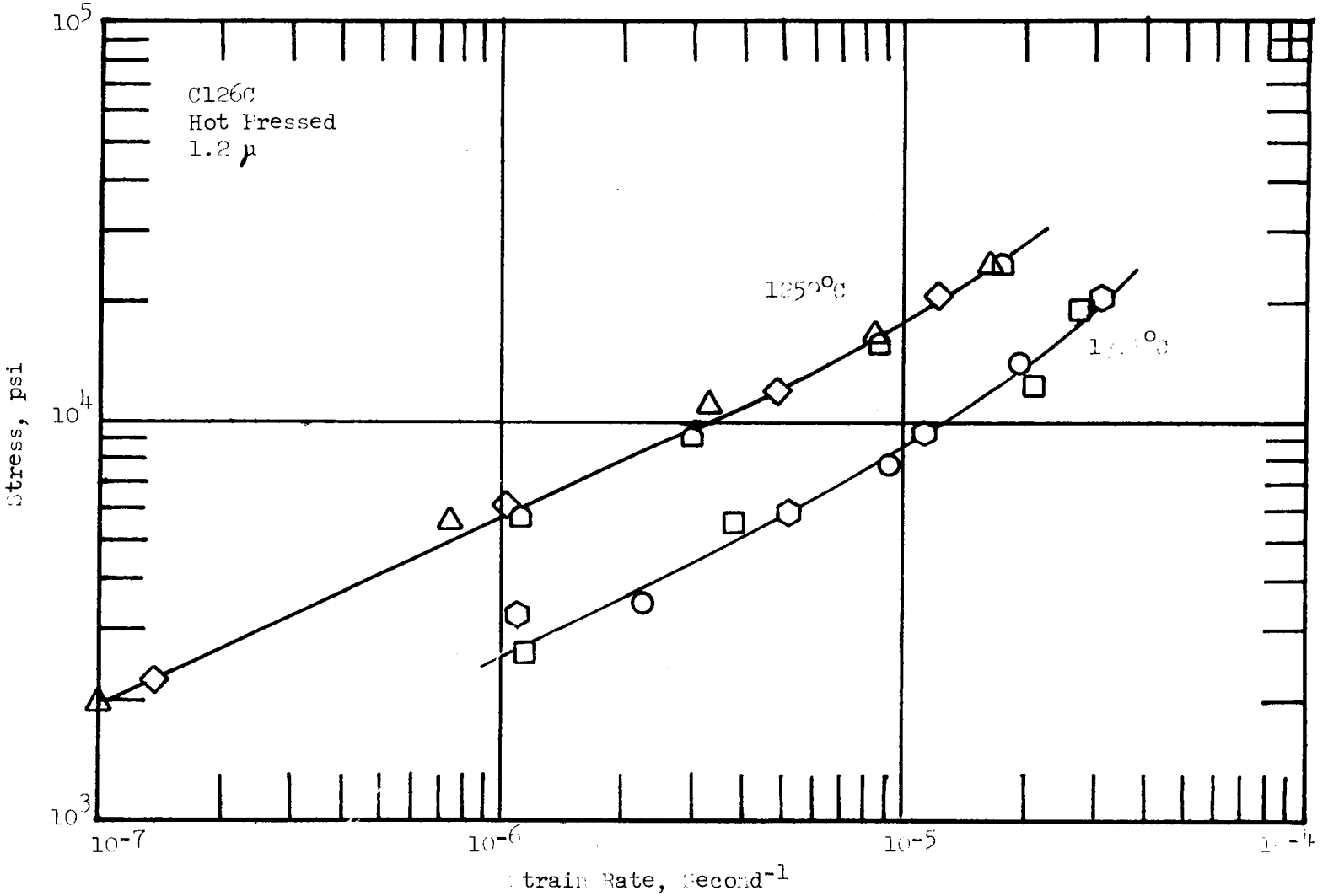

Figure 4. Flo tress- train Rate Behavior of Hot Pressed Material, C1 , Te te in Air. The stresses were calculated usi the elastic formula.

the resultant slope would be between 0.5 and 0.6 indicating that the uncertainty is in the increase in rate sensitivity to near unity, not in the existence of the non-Newtonian region.

A second source of error is from grain growth during tests which for most of the probable deformation mechanisms would cause an increase in flow stress. For the tests at 1313°C and below, the difference in grain size of specimens tested rapidly at high rates and those in long tests starting at low rates was generally less than 10%. Although grain growth could also contribute to some of the apparent change in behavior, comparison of the specimens started at different initial rates again indicates the effect to be real, although the apparent magnitude could be increased by these two problems.

For the tests at 1400°C and above, grain growth was more severe; some of the specimens from long tests at 1400°C and from 1490°C had grain sizes of 2 μ or above. The data from specimens which had severe grain growth problems suggested a sigmodial stress-strain rate curve with an initial region of high apparent rate sensitivity decreasing with increasing strain rate and then apparently increasing again. It is thought that this first region is an artifact resulting from grain growth; this would be more severe at the low rates where the time for each test is longer. Some additional tests were performed at 1400° or 1418°C, shown in Figure 5, in which the tests were started at higher rates and the rate was lowered into the range where the high rate sensitivity had appeared. These results tend to confirm that the apparent shift at low strain rates was an anamoly caused by concurrent grain growth. Correction of these data for grain growth was not warranted since the time dependent grain growth law was not known for this material and, further, because any shift in mechanism may involve a change in grain size dependence on flow stress. Further investigation for a low rate transition at lower temperatures was not possible with the present apparatus because of the low strain rates required.

Graphical reduction of the stress-strain rate curves was made using eqn. (2) and neglecting horizontal load effects on the bending moments. The results are in Figure 6 which also includes the data for the high purity material. Because of the less accurate deflection measurement in the air furnace, the points at 10^{-7} sec^{-1} for the air tests were not included in the corrected curves. The correction is a graphical one for each curve in Figures 3 and 4 and so the individual data points are not presented in Figure 6. The sigmodial curve shown in Figure 3 for 1418°C was converted directly for comparison. However, the other curve at 1418°C with a single slope increase was obtained by assuming grain growth problems for the long tests and emphasizing the initial test points and bars started at higher rates, which had little grain growth. This curve was used for the subsequent analysis of the data. No reduction of the 1490°C data was performed.

It can be seen that the corrected curves give a stronger indication of a transition in behavior from a mechanism with $m = 0.5$ to one with $m = 1$. However, further testing at lower rates would be necessary to be certain that m has reached a lower limit at 0.5. Again the similarity in behavior of the doped material and the high purity Al_2O_3 can be seen. This suggests that further testing of the high purity material at lower rates may reveal

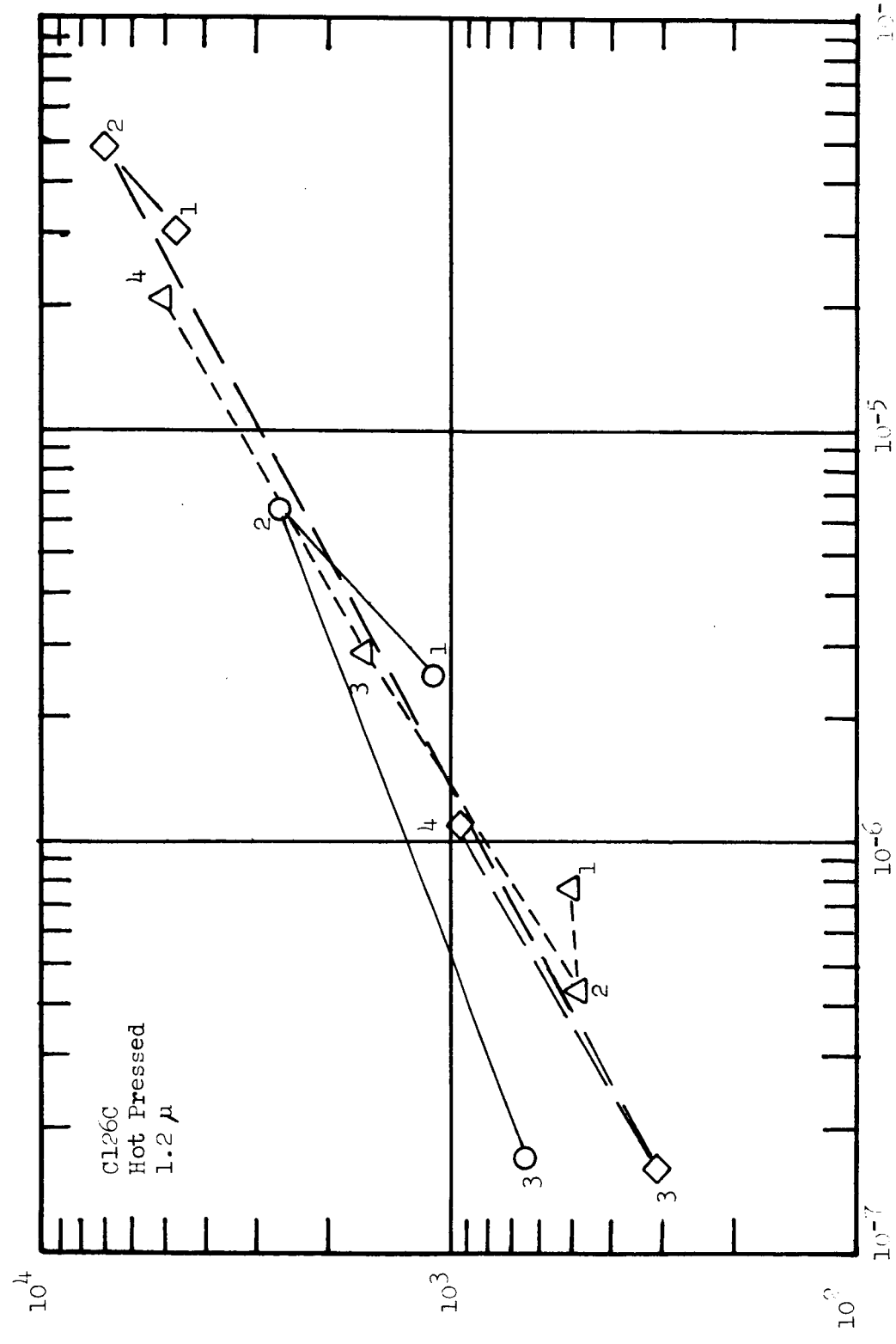

Figure 5. Stress- train Rate Curves of C126C Bars at 1400° and 1416°; showing the effect of Reducing the train Rate. The stresses were calculated using the elastic formula. The numbers next to each point refer to the actual order of testing.

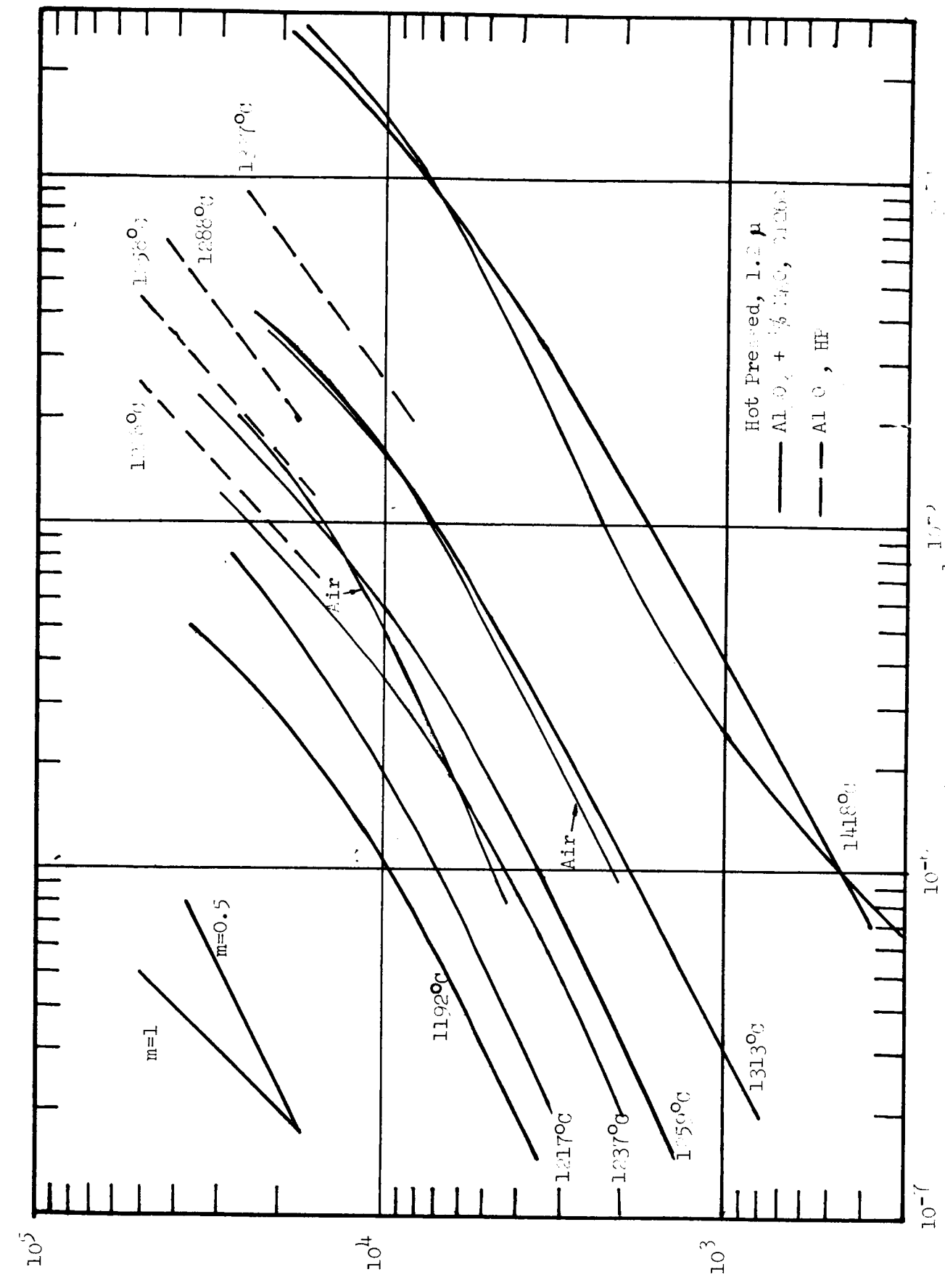

Figure 6. Corrected stress- strain rate curves for [illegible] and HF materials.

a similar transition. The high purity curve with the most extensive data was that at 1228°C; because this material had a higher fracture strength, data could be obtained up to 45 Ksi which allowed a better confirmation of the high rate sensitivity range. The slope averaged 0.93 for this line[2a]. This indicates that without a transition in behavior for one or both of these materials, the two stress-strain rate curves would simply cross each other which seems highly improbable.

Activation energies were obtained by plotting $\dot{\epsilon}$ vs. 1/T at several stress levels as shown in Figure 7. The high purity data are included in this plot as are points from a few small C126C bars tested on the same apparatus as the high purity bars to check calibration.[2a] The data suggest a change in activation energy between the high and low stress regions indicating ΔH is about 100 Kcal/mole for the high stress Newtonian region and about 115 Kcal for the low stress region. This is not a large difference, but the consistent change with stress tends to give credability. It is seen that the high purity bars indicate a somewhat lower ΔH, but that the fit with the C126C data is quite good, considering testing was in a different apparatus and small differences in grain size may exist. A similar plot at 5000 psi for the C42 data gave a value of 114 Kcal/mole. This is similar to the values at low stresses for C126C material which is consistent since this material exhibited a rate sensitivity of 0.67 over the limited range in which it was tested. Also, previously reported data[3] on Al_2O_3 + $\frac{1}{4}$% MgO with grain sizes of 1.8 and 2.0 μ and average m = 0.63 had activation energies of 117 and 119 Kcal/mole.

Since testing at the same temperature was not possible for all the materials, grain size comparison is made by extrapolation of the $\dot{\epsilon}$ - 1/T data to an intermediate temperature, 1528°C. All of the data were for 5000 psi. The results, including the sintered bars from last year[1] and earlier data[3] are in Figure 8. The data appear to fit two separate lines suggesting a consistent calibration difference between the two studies rather than an atmosphere or purity difference as was inferred in the previous report.[1] The recent work covers materials tested in three different furnaces, and in both air and argon, and shows good internal consistency and so the absolute magnitude of this data is more likely correct. A straight line fit to this data indicates an $\dot{\epsilon} \propto G^{-2.7}$ dependence. Although this would appear to suggest diffusional creep with a shift to domination by grain boundary diffusion at the finest grain sizes, the effect of the non-Newtonian mechanism must also be considered in a complete interpretation of this result.

B. Crystallographic Texture

A strong basal texture, with the c-axis parallel to the forging direction, has been reported in Al_2O_3 heavily forged at high temperatures[8,9] and has been attributed to basal slip during forging. In addition, a strong texture was found[1] in a specimen forged 38% at 1450°C and at relatively low stress; appreciable cavitation in this specimen, JC-1474, reduced the density to 93.3% after forging. To further assess the contribution of basal slip in deformation at low stresses and intermediate temperatures, orientation was measured in two additional specimens. One was the previously[1] reported JC-1469, forged 16% at 1450°C and 4 x 10^{-5} sec^{-1} which had a final density of 99.3%. A second specimen, C126-4U, was prepared by creep forging a piece of the C126C

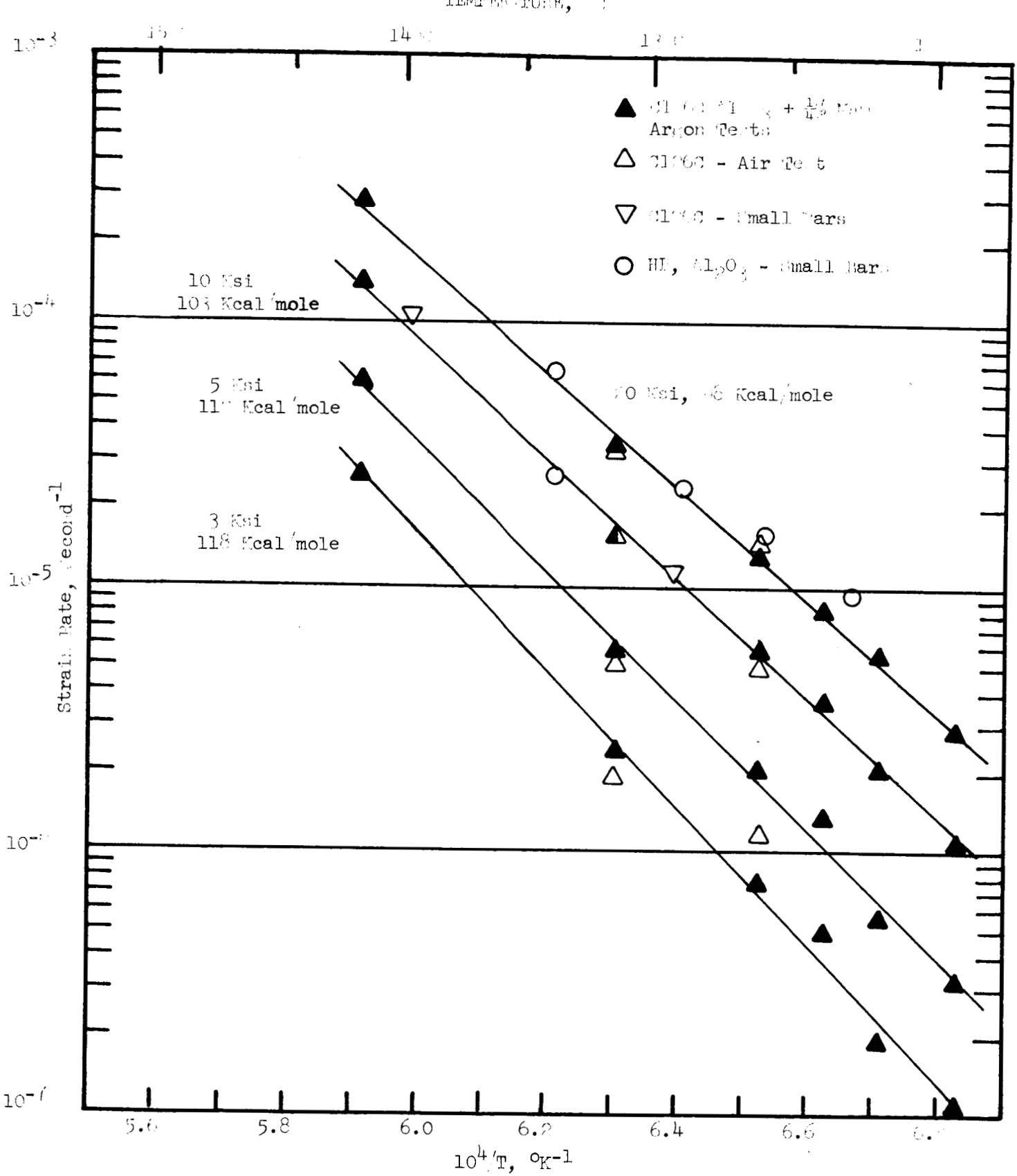

Figure 7. Strain Rate versus 1/T Showing the Activation Energy for Deformation for the C126C and HP Materials.

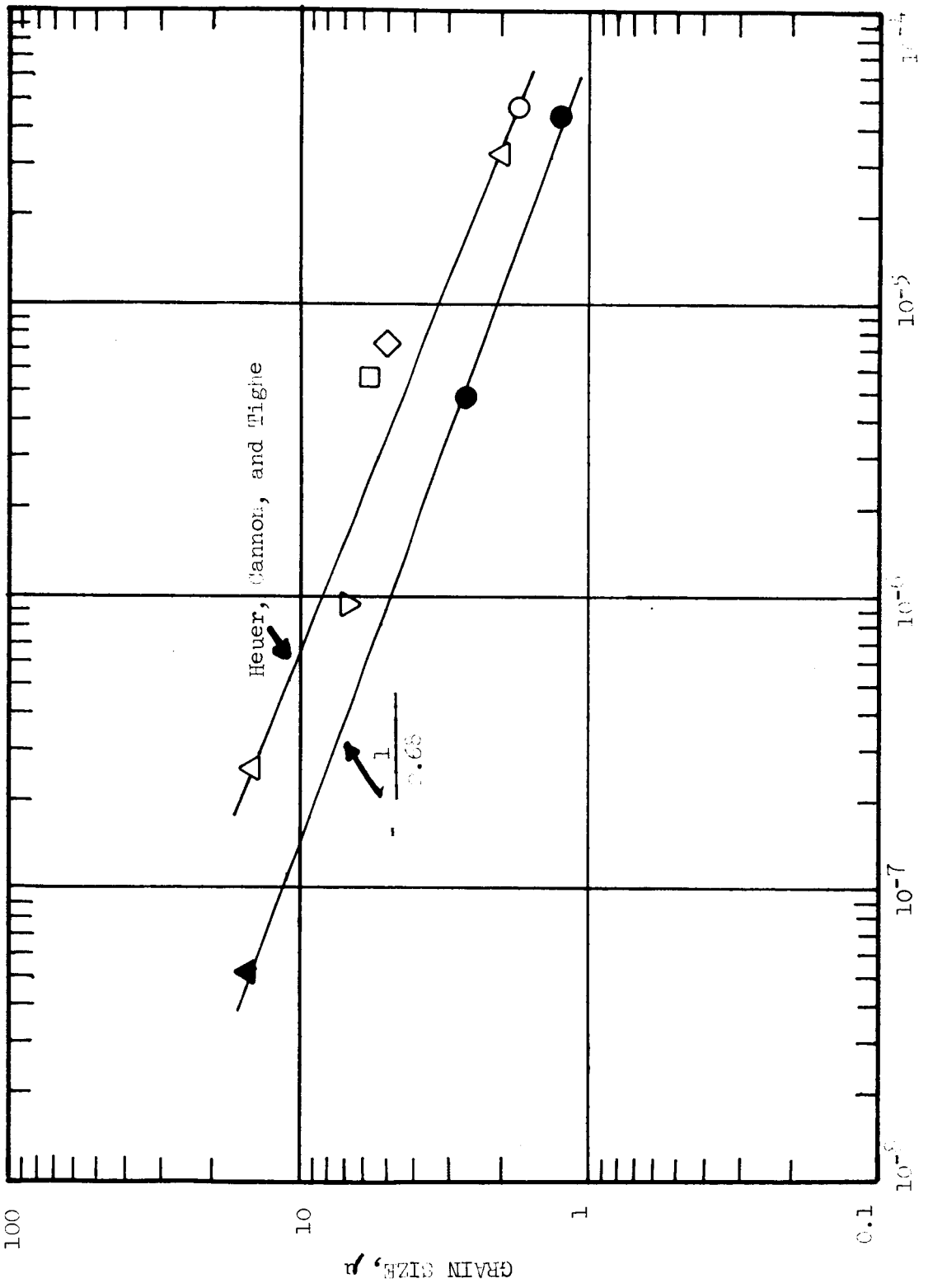

Figure 8. Plot of the strain rate dependence on the Grain size for various materials at 5000 psi and 1580°C.

material at 1315°C and at an average strain rate of about 2×10^{-6} sec^{-1}. A small specimen was compressed under a dead load giving an initial stress of 4100 psi which dropped to 2800 psi as the piece reached an ultimate strain of 31% reduction. After forging, the piece had a density of 99.9%, indicating little cavitation occurred. The dead load testing was necessitated by the slow strain rate which was selected to be below the apparent transition seen in the flexure test and to be at a stress below that reported for basal yield in sapphire at comparable or lower strain rates. In order to achieve the necessary stresses in the available creep unit, a small specimen of dimensions 0.10 x 0.19 x 0.20 inch was used; the elongated cross-section was selected to facilitate X-ray orientation measurements.

These specimens were analyzed for preferred crystallographic orientation by an X-ray diffraction technique which has been developed and used on previous programs[10,11]. The crystallographic texture can be described by what is essentially an azimuthally averaged, inverse pole figure. In this procedure, the relative population density of different planes is plotted against the angle between these planes and the basal (000.1) plane. With proper normalization, this is then also a plot of the population density of the basal planes at the same angle from the reference surface.

Experimentally, the procedure is simple. The diffraction pattern of a randomly oriented (powder) sample is obtained. Values are calculated of $P_o(hk.l)$ defined by the relation

$$P_o(hk.l) = \frac{I\ (hk.l)}{\sum_{hkl} I\ (hk.l)}$$

where I (hk.l) is the diffraction peak intensity for reflection from the (hk.l) plane. Similarly, the diffraction pattern of the forged body is obtained using a face perpendicular to the pressing direction taken at the mid-plane of the piece. Values of P (hk.l) are calculated as before, and then the ratios $R(hk.l) = P(hk.l)/P_o\ (hk.l)$ are calculated. These values of R are plotted against θ, the angle between the plane hk.l and 00.l.

In the case of a random (powder) sample, R has the constant value of unity. In the case of a perfectly oriented sample, R is zero everywhere except at $\theta = 0$ where it has some large finite value. In the case of a distribution of orientation, R will, in general, decrease monotonically from $\theta = 0$ to $\theta = 90°$. The better the alignment of the crystallites, the greater will be the intercept at $\theta = 0$ and the steeper the drop with increasing θ.

The results are shown in Figure 9. The results for JC-1469 forged only 16% indicate that texture is just beginning to develop at this strain. Unfortunately, the plane at 0° has a low X-ray intensity and so is the most difficult to measure accurately; the values for the planes at 18° and 90° are similar to those reported[8] for high temperature forgings where only slight texture was found at strains below 20%. The lower temperature piece, forged 31%, shows decided basal texture, although it is not as strong as found for the previously[1] reported piece forged 38%. These results indicate that basal slip is active in the intermediate temperature deformation of Al_2O_3 even at low strains and that it does not simply occur at high strains and concurrent with significant cavitation.

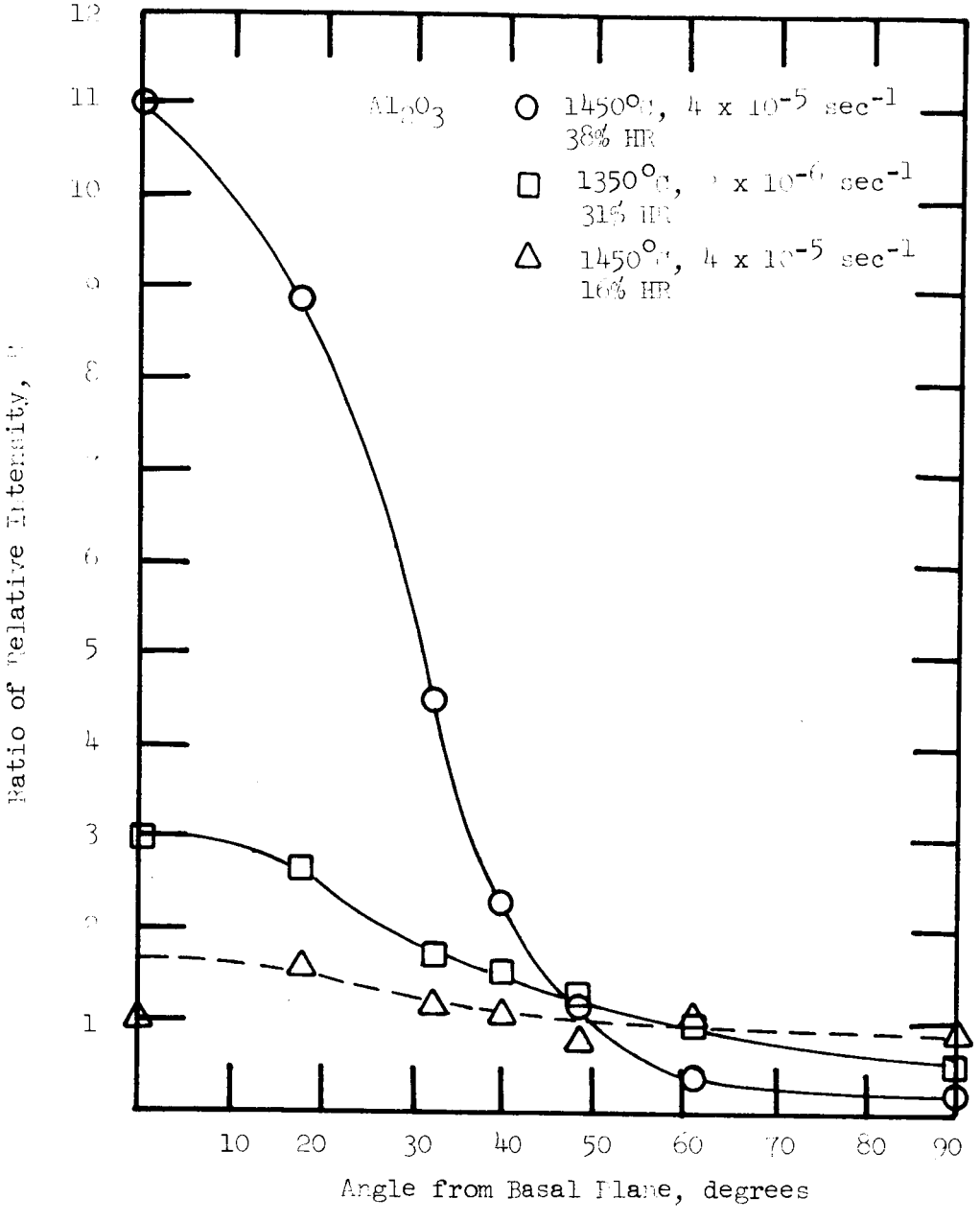

Figure 9. Ratio of Relative X-ray Intensity for Compression Specimens Showing Basal Texture. The data from the 38% HR from last year is included for comparison.

C. Hemisphere Forgings

Two additional attempts were made to deep draw hemispheres from flat, 3-inch diameter blanks of alumina. The procedure was similar to that previously used[1], but with a new graphite punch and die which had a hemispherical radius of 1.05 inch. For the first one the die had an entrance angle of 30° and a small entrance radius compared to the previously used set-up[1] which had a 40° entrance angle and generous radius. For the second, the die entrance radius was increased to prevent cracking.

The first forging, D1600, used a blank with an initial grain size of 2.4 u and was done at 1575°C to reduce the amount of grain growth during the deep drawing. The blank broke into several pieces as can be seen in Figure 10. The primary radial cracks clearly occurred quite early in the test, and appeared to originate in the flat part of the crack between the two largest pieces. It was not clear exactly where in this region the crack started. It seems likely that the initial crack may have resulted from a brief increase in strain rate and load during the early part of the test. A second set of cracks also developed at the die entrance region where the maximum bending occurs. These appear to be the result of drawing over too sharp a radius at too high a rate.

Examination of the surfaces of this forging indicated some undesirable chemical compatibility problems. Spots of a molten phase could be seen on the surface; this may be B_2O_3 from the BN lubricant used. It is not known whether the oxide was initially present in the BN or formed during forging. This must be prevented since attack by a liquid phase could lead to cracking during forging.

The second forging, D1762, was planned to have a reduced strain rate in the initial stages, because of the early cracking of D1600 and because the earlier hemisphere[1], D1442, had some tearing at the apex; this tearing was not in the region of maximum thinning strain and so appeared to have been caused by excessive strain rate in the initial part of the drawing. The temperature for this forging was 1600°C.

This blank also cracked very early in the run; the deflection was only about 0.04 inch compared to the blank thickness of 0.068 inch. The run was terminated in order to try to establish the cause of premature failure. The fracture occurred rapidly and at a relatively low load. The forging had been in progress for more than an hour and the deflection was significantly less than had been calculated for the loading to obtain the target strain rate of 2×10^{-5} sec^{-1}. At the failure load, an approximate calculation of the maximum bending stresses at the center of the blank gave 12 Ksi; the calculation does not include stretching stresses which should not be large at that stage of deflection or contact stresses under the punch. This value of fracture stress is lower than expected (see the next section for further discussion of fracture strength). A contributing cause is that the stress is biaxial tension; at low temperatures, a reduction of fracture strength under biaxial loading of about 20% has been reported for Al_2O_3[12]. At high temperature, a similar effect may be anticipated in the brittle regime and reduced fracture stresses for plastic tearing under biaxial loading are also probable.

The failure started at the center and propagated outward with several

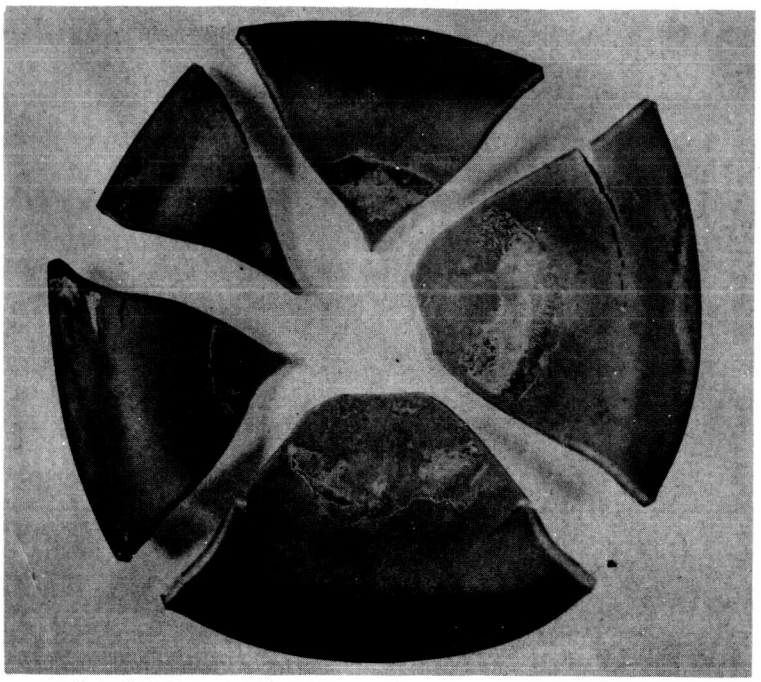

#5531-1 1X

Figure 10. Cracking of Deep Drawn Al_2O_3 Hemisphere, D1600. The upper and right pieces should be interchanged.

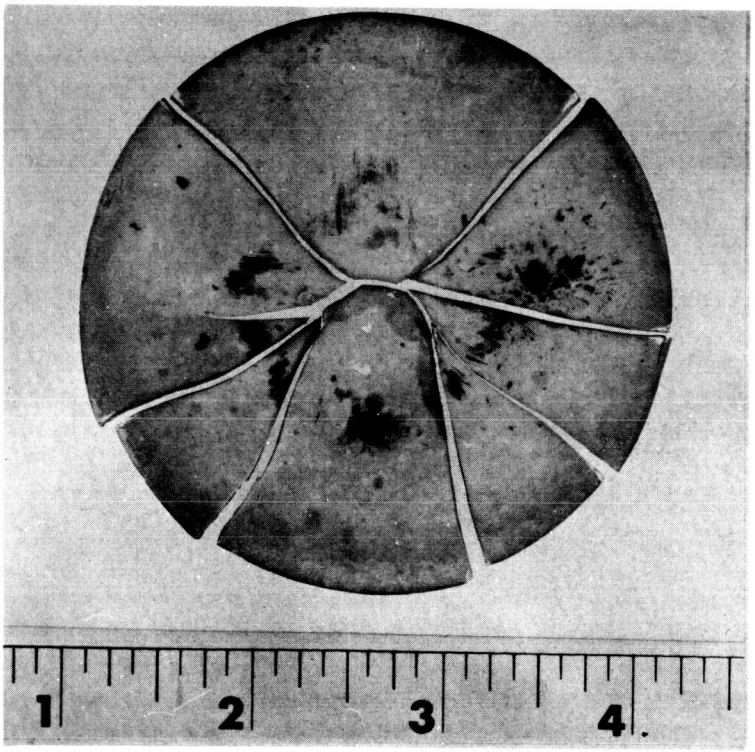

#5603-1 1X

Figure 11. Premature Cracking in Hemisphere Run D1762. Most of the observable bending occurred after fracture.

branches as seen in Figure 11. Examination of the fracture surfaces confirmed that the crack started in the center of the disc. However, it was surprising that the origin, as shown in Figure 12, appears to be at the surface on the punch side, which would be in compression from bending. In fact the plane of the crack was parallel to the scratches on the punch side from surface grinding the blank. Even if stretching stresses were appreciable, the higher tensile stresses would still exist on the opposite side of the plate. This suggests that contact stresses under the punch were important. A possible explanation is that the low deflection rate may have resulted from punch hang-up and that when the punch loosened, the transient increase in load was sufficient to initiate fracture.

Microstructural examination of the previous[1], more successful hemisphere, D1442, done at 1625°C, and of highly strained areas in D1600 was performed using electron microscopy of replicas combined with some light microscopy. For D1442, the as-forged hemisphere was etched in phosphoric acid and the inner and outer surfaces were replicated. A typical region from the outer surface is shown in Figure 13a; it can be seen that appreciable grain growth occurred. The average was 6.8 μ compared to an initial size of 3 μ for this piece. The grain size of D1600, done at 1575°C, only increased from 2.4 μ to 3.8 μ.

On D1442 many small spots could be visually seen on the O.D.; replication showed that these were small coarse-grained patches. The grains in these patches were about 30 μ as can be seen in Figure 13b. These coarse grained regions acted as hard spots and did not deform as fast as the surrounding regions. Some cracking was observed in the regions immediately surrounding the hard spots which presumably resulted from the higher local strain rates. Similar coarse grained patches as shown in Figure 14 were also seen in D1600. Because there was less thinning of this piece, these spots did not stand high on the surface as in D1442. It is presently thought that these coarse grained patches are in the original blanks.

A core of hemisphere D1442 was taken near the apex in the region of greatest thinning strain. This area had experienced an average biaxial bend strain of 3.9% and a thinning strain of 9.9%. Using the usual equivalent strain formula:

$$\bar{\epsilon}^p = \sqrt{\frac{2}{9}\left[(\epsilon_1^p - \epsilon_2^p) + (\epsilon_2^p - \epsilon_3^p) + (\epsilon_3^p - \epsilon_1^p)\right]} \qquad (4)$$

the total equivalent strain was calculated to vary linearly from 2.2% at the I.D. where the bending and thinning strains cancel, to a maximum of 17.6% at the O.D. These values are approximate in the sense that they only represent the final average strains and do not account for any redundant strains in the actual deformation.

Micrographs are shown in Figures 15, 16, and 17 of typical regions in the cross-section from near the O.D., from the center, and near the I.D., providing a scan along the strain gradient. These show an increase in the amount of grain boundary cavitation with the increase in strain. The difficulty in assessing the actual amount of cavitation can be appreciated by comparing the as-polished and the etched views. It is obvious that etching

#5603-2 15X

Figure 12. Fracture Surface of Crack Showing the Apparent Origin on the Surface Under the Punch.

#71457 (a) 1500X

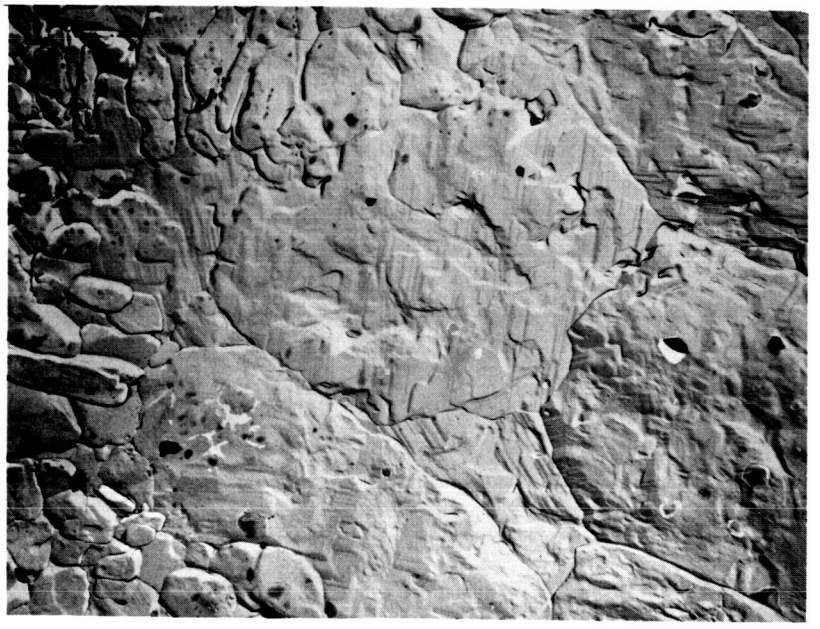

#71458 (b) 1500X

Figure 13. Microstructure of Outside Surface of Hemisphere D1442 Showing a Typical Area (a) and an Area at the Edge of a Coarse-Grained Patch (b).

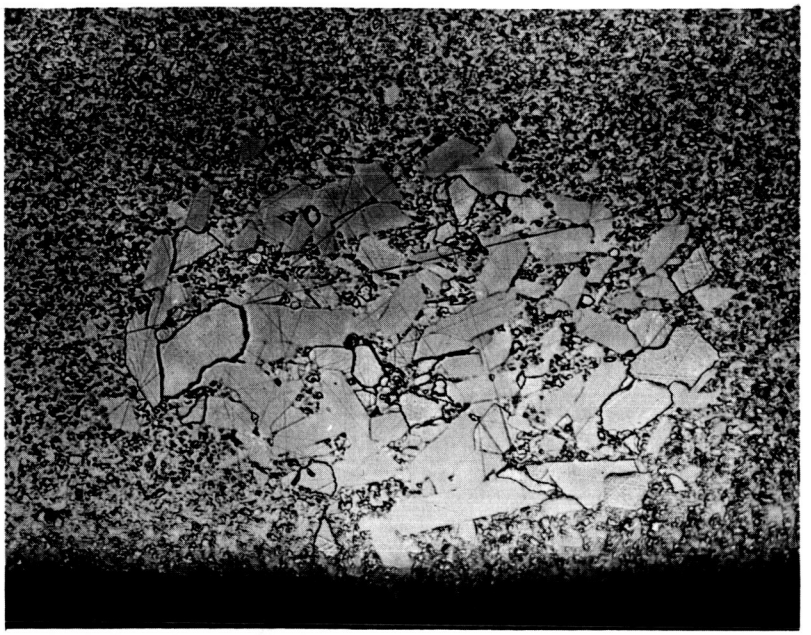

#5531-3 250X

Figure 14. Coarse-Grained Patch from Piece of D1600.

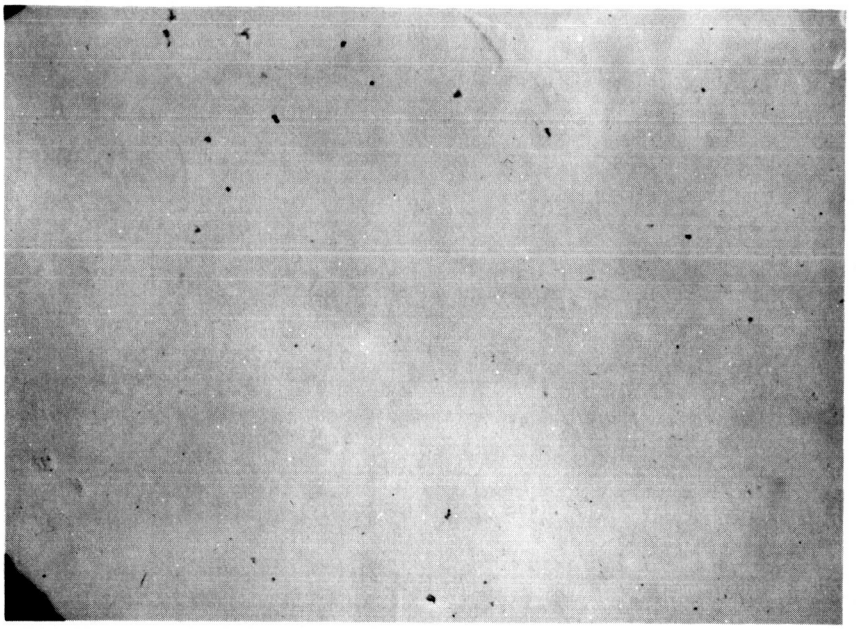

72297 (a) 1500X

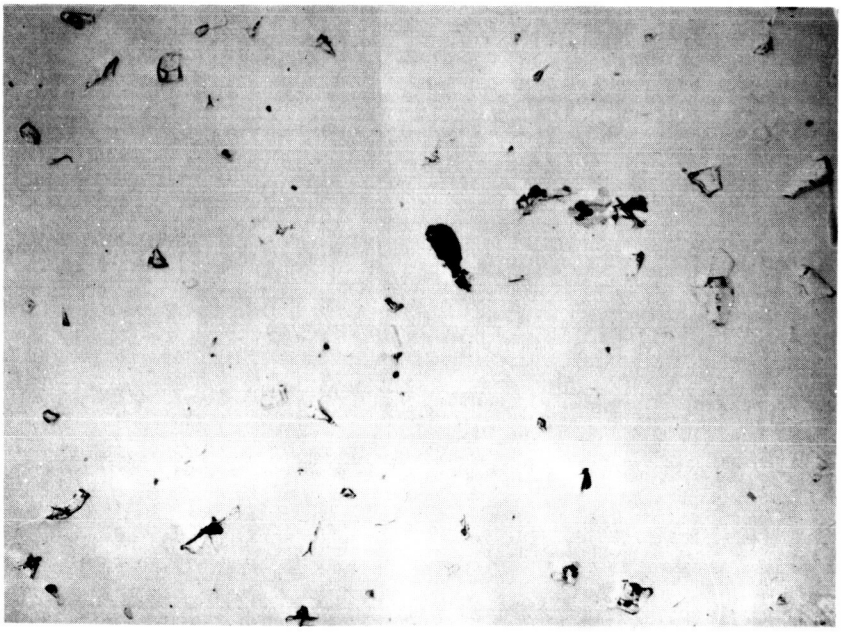

72305 (b) 1500X

Figure 15. Cross-Section of Hemisphere D1442 Near the O.D. in the (a) Polished, and (b) Polished and Etched Condition.

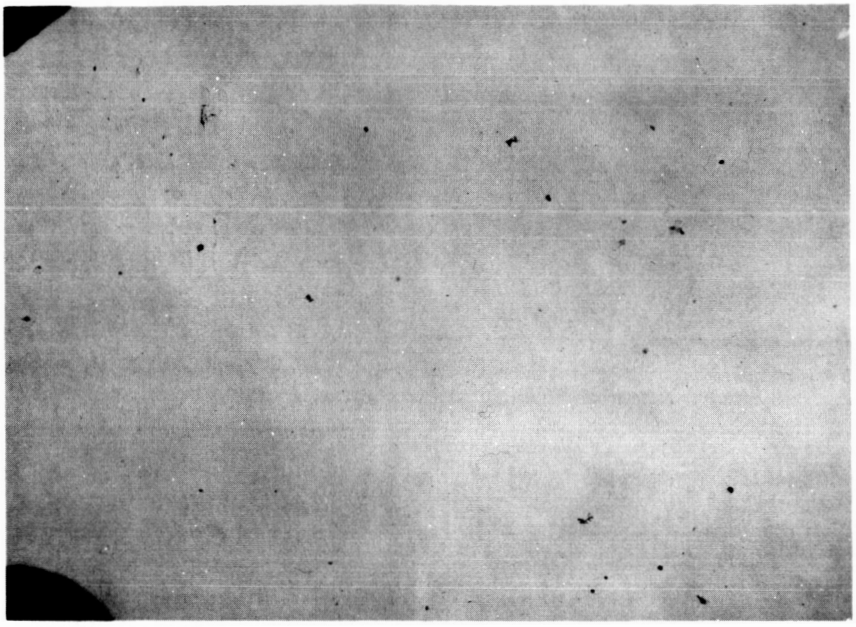

72296 (a) 1500X

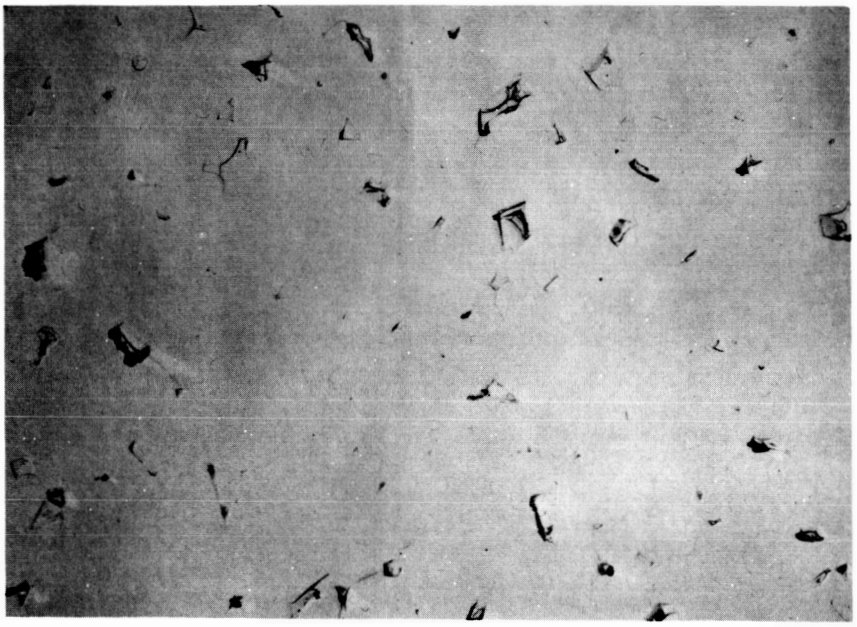

72307 (b) 1500X

Figure 16. Cross-Section of Hemisphere D1442 from the Center Region in the (a) Polished, and (b) Polished and Etched Condition.

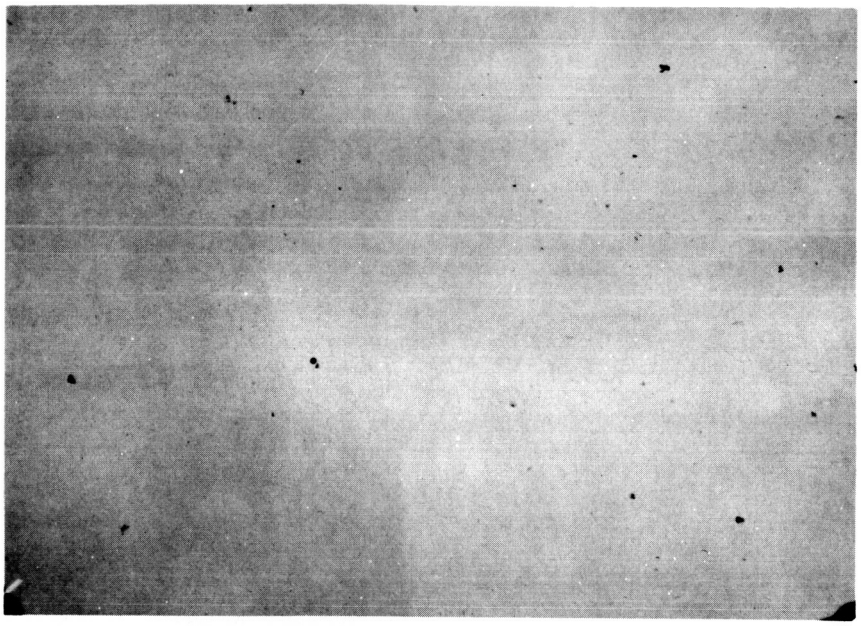

72295 (a) 1500X

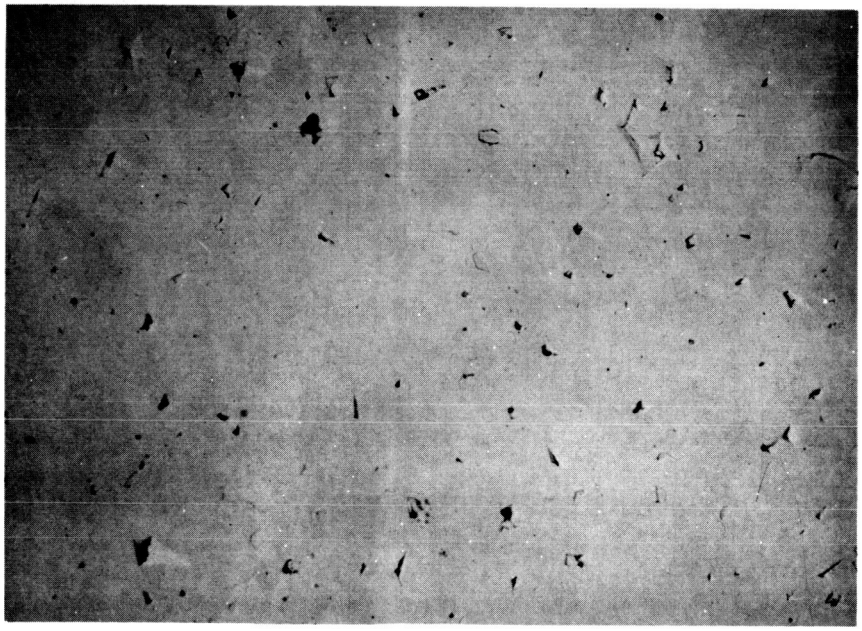

72306 (b) 1500X

Figure 17. Cross-Section of Hemisphere D1442 Near the I.D. in the (a) Polished, and (b) Polished and Etched Condition.

significantly increases the apparent amount of porosity. This likely occurs because the triple points have fine porosity which is not apparent in the as-polished condition, but other factors such as higher residual stress at the points of constraint to grain boundary sliding or impurity accumulation could also contribute. Most of the cavitation is at triple points rather than along grain faces. Most of these cavities were still quite isolated at this stage, except at the surface in or near the coarse grained patches. An example of how they can grow and connect to form larger cracks is shown in Figure 18 taken from a coarse grained region. Areas from regions of high bending strain in D1600 exhibited similar cavitation.

In these several forgings, tearing or cracking has been caused by several factors. Apex tearing, or even rapid fracture has been frequent and is thought to be caused by excessive strain rate or strain rate fluctuations during the early part of the forgings. Similar problems in the skirt can also be caused by an excessively sharp die entrance radius. A second source of cracking has come from coarse grained patches in the blanks; these act as 'hard' spots and can cause tearing in the regions of strain concentration around them. At these high temperatures there are also chemical problems. Grain growth on the I.D. of D1442 apparently resulted from interaction with the graphite lubricant used on the punch. This problem has not been observed when using a BN coating, but occasional problems of interaction with BN or B_2O_3 formation have appeared. By eliminating these specific problems then grain boundary cavitation will become the limiting feature; further optimization of the temperature strain rate schedules will be required to further minimize or eliminate it. It appears to be important to achieve smooth load application to prevent transient load or strain rate increases which can cause crack formation.

D. High Temperature Fracture

Successful forging of these rate-sensitive ceramics requires careful control of the applied loads to achieve the desired strain rates without developing stresses high enough to cause fracture. However, to minimize forging times and grain growth, it is desirable to forge at the highest rates possible without incurring fracture or excessive cavitation. To indicate allowable stresses over the temperature range of interest, 1400° - 1900°C, the reported fracture stress versus temperature data for polycrystalline Al_2O_3 have been collected and are plotted in Figure 19. Most of the fracture studies were conducted at temperatures below the present range of interest, and the concern was primarily with short time fracture; the lines from Spriggs, Mitchell and Vasilos[13] are typical of these results. In order to supplement these data and to further indicate the effects of plastic deformation, the data from three previous studies of flow stress-strain rate were reviewed.[1,3,14] Most of these data are plotted as individual points indicating either fracture or the highest flow stresses which were achieved in specimens where fracture did not occur. In some cases, these highest stresses were well below the expected fracture stress. These data cover a range of grain sizes from 1 to 15 μ and strains at failure as high as 3%. The line marked high purity represents a similar compilation[2] of short time and plastic test results for the 1.2 μ high purity Al_2O_3. The data for C79 were the average of several tests at fast enough strain rates to cause brittle fracture. Also plotted are the highest flow stresses reported by Folweiler[15] in similar stress-strain rate tests for material of 7 to 30 μ grain size; fracture was reported

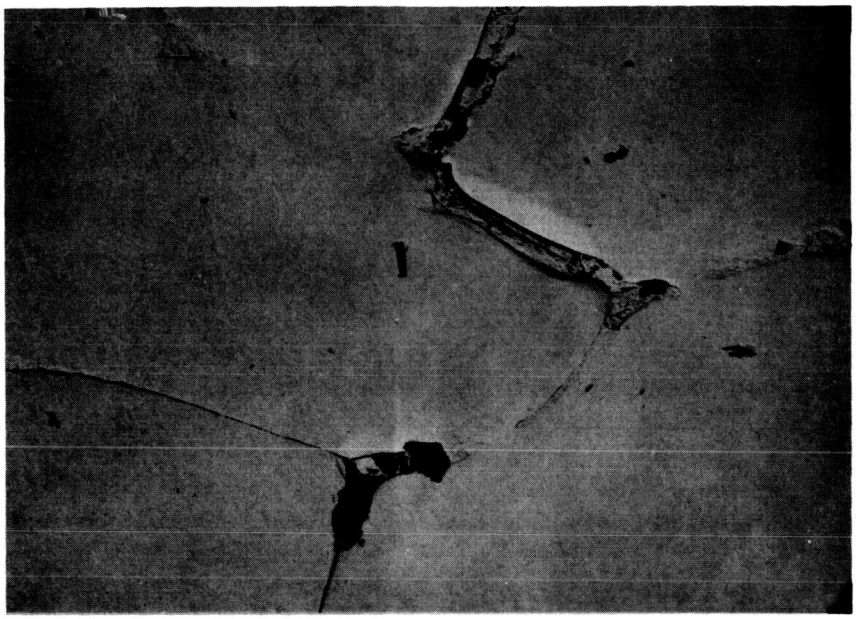

72299 3000X

Figure 18. Development of crack from growth and connection of triple point and grain boundary cavities; in large grain region near the surface of hemisphere D1442.

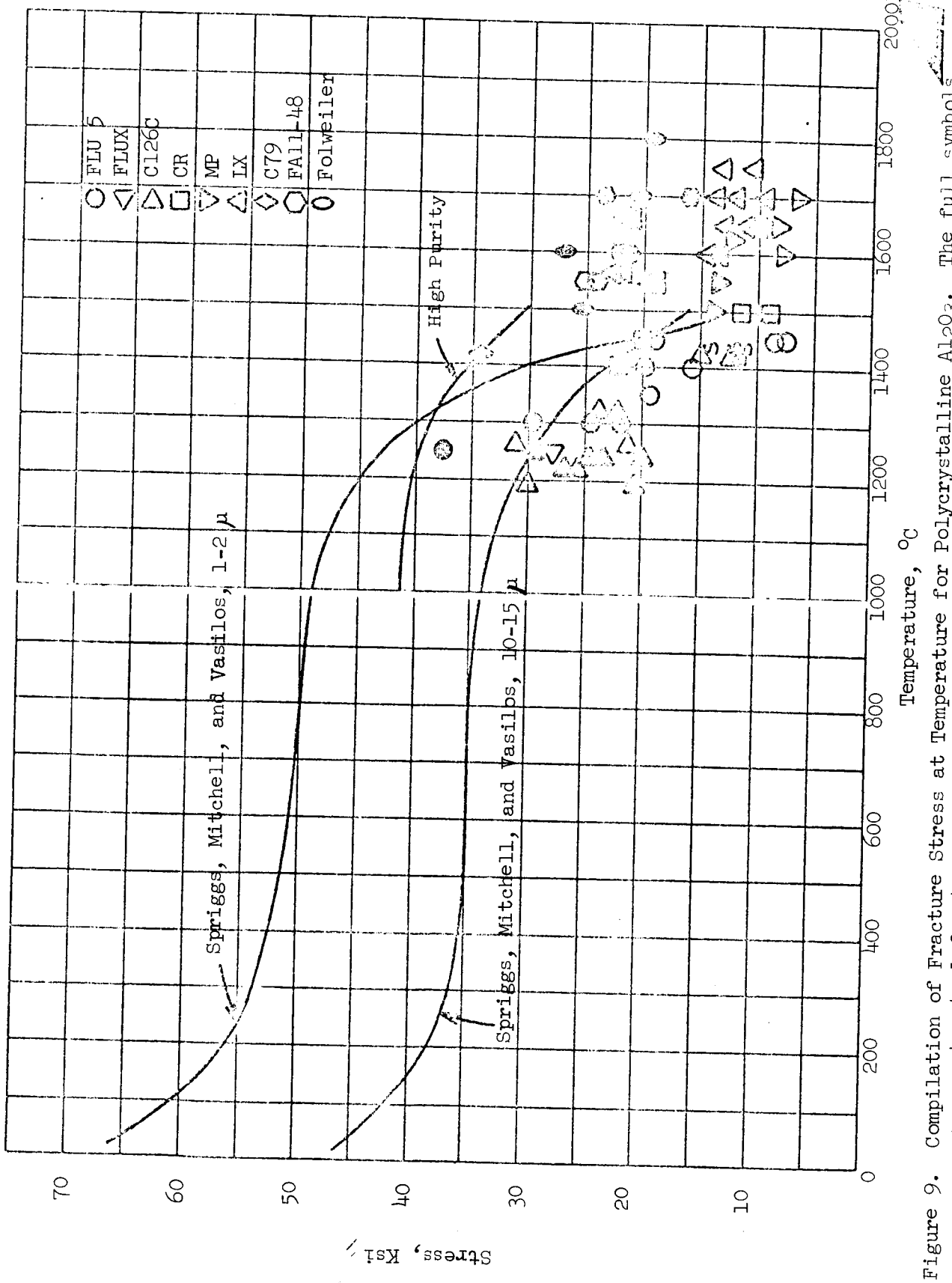

Figure 9. Compilation of Fracture Stress at Temperature for Polycrystalline Al_2O_3. The full symbols represent actual fracture and the open symbols represent achievement of steady state creep without fracture. The 's' represents the stress at which slow crack propagation began in multiple bend tests. (Data from Refs. 1-3, 13-15).

to occur at these highest points in this study.

These data indicate a rather broad range of fracture stresses which is not surprising considering the range of grain sizes and strains before failure which are included. At high temperature, the fracture behavior can be divided into two broad categories. At sufficiently high stresses, the fracture is rapid and the fracture surfaces are brittle in appearance. This behavior can qualitatively be considered in terms of a Griffith fracture criterion, in the sense that rapid fracture occurs when the flaw size becomes critical. Where plastic flow is occurring, the critical flaws may develop as a result of growth of intrinsic flaws or grain boundary separation before the rapid crack propagation stage.

A second mode of fracture is also seen where a significant amount of stable crack growth occurs by tearing during plastic deformation. At lower stresses or where stress gradients are high, this stable growth can be an appreciable fraction of the cross-section before rapid fracture occurs. This type of behavior was seen in the multiple bend tests reported last year and in local tearing seen in forgings.[1] At high temperatures, the distinction between these two modes is partially qualitative since at intermediate rates the intrinsic flaws may be enlarged by a small amount of stable growth. In general, however, a significant difference exists in the fracture surface appearance between the two modes, and significant plastic flow can occur concurrent with the slow crack growth. The stresses at which observable cracks developed in the multiple bend tests reported last year[1] are also shown. These results suggested a strong stress-dependence and showed that significantly higher strain could be obtained at lower strain rates, with the commensurately lower stresses, before crack growth became significant.

III. DISCUSSION

The deformation kinetics and microstructural features observed for Al_2O_3 indicate that several mechanisms are involved and may influence the limiting kinetics over the range of temperature, strain rate, and grain size investigated. The important features which must be considered are:

1. The strain rate sensitivity of 15 μ material is near m = 1, but as the grain size decreases, there is increasing appearance of non-Newtonian behavior. At 1 μ, the data indicates that m = 0.5 or perhaps lower at low strain rates, but that with increasing stresses m approaches unity. This transition to a higher rate sensitivity at high stresses suggests two coupled mechanisms are involved with the rate limited by the slower one.

2. A strong grain size dependence exists; as shown in Figure 8, at 1528°C, the average behavior fits a dependence of $\dot{\varepsilon} \propto G^{-2.7}$. This experimental value would approach 3 at lower comparison temperatures or would be smaller if the data were extrapolated to a higher comparison temperature. Further, it is sensitive to the stress selected because of the non-Newtonian behavior of the fine grain material which causes a higher apparent exponent at higher stresses.

3. The apparent activation energy for creep shows a dependence on grain size with a value of 132 Kcal/mol for the 15 μ material and lower values for the finer materials. There is an indication that the high stress, Newtonian region has a lower activation energy, about 100 Kcal/mol than does the non-Newtonian, low stress region where it is about 115 Kcal/mol.

4. A crystallographic texture develops in compression to high strains with alignment of the c axis parallel to the compression direction. This has been found in fine grained materials at temperatures of 1315° and 1450°C and low strain rates. For the two specimens at 1450°C, the maximum shear stress, taken as $\sigma/2$, was about 3000 psi during the tests, which is between the critical resolved shear stress for upper and lower yield for basal slip in sapphire.[16,17] For the specimen at 1315°C, the maximum shear stress decreased from 2050 to 1420 psi during the creep deformation, which is below the CRSS, of 2300 psi, for lower yield for basal slip of sapphire at the same temperature and strain rate[17] and is even below the so-called creep yield value of 2030 psi from Wachtman and Maxwell's tests.[18] The texture increases with strain being barely apparent at 16% reduction and strong by 38% reduction. Texture has also been reported[8,9] in coarser grained Al_2O_3 at higher temperatures, but these studies started with fine grained preforms which experienced grain growth and sometimes even recrystallization during forging so it is uncertain whether there is an effect of grain size on texture formation.

5. There is extensive microstructural evidence[1,2,3] for grain boundary sliding in the fine grained material. Electron microscopy shows offset triple points, broad, distorted, and sometimes wavy boundaries, displacement of grains out of the surface, grain boundary cavitation, and occasional alignment of boundaries for several grains which

would allow easier shear. There are occasional indications of slip such as surface steps, steps in grain boundaries, and low angle boundaries. Transmission microscopy[3] indicates some grain boundary dislocations, and few lattice dislocations, suggesting the boundaries to be the principle sources and sinks for dislocations. At high strains there is some indication of grain elongation.

6. Over the range of grain size investigated, grain boundary cavitation is often seen, especially at triple junctions. At a given stress and temperature, the cavitation increases with strain, but the overall experience suggests that the amount of cavitation is lower at lower stresses or strain rates. Void formation is less in compressive modes where the hydrostatic pressure is higher.

7. Over the conditions investigated, a steady state stress appeared to exist for constant strain rate conditions and no substantiated indication of work hardening was found. Significant indications of apparent strain hardening were always found to have been accompanied by grain growth, and the amount of hardening could be reasonably well accounted for by the grain growth. Where grain growth is slow, it may be enhanced by the concurrent strain,[1] but at higher temperatures it may be rapid enough that the strain enhancement is not important.

8. For the materials tested, little apparent effect on deformation of specimen composition or test atmosphere was found. Most of the material had $\frac{1}{4}\%$ MgO which is above the solubility limit resulting in occasional small grains of spinel. For the 1 μ material, there was no apparent difference between the doped Al_2O_3 and a higher purity material without MgO. There does, however, appear to be an increase in fracture strength and a reduction in the amount or rate of cavitation for the higher purity materials.

The regions of linear stress dependence, the strong grain size dependence, and the activation energies near those for self-diffusion suggest diffusional creep to be one of the important contributing mechanisms as has been suggested by previous investigators.[14,19] It has recently been suggested by Ashby[20] and others[21-23] that, under some conditions, diffusional creep may become interface reaction limited with the boundaries no longer acting as perfect sources or sinks for point defects; this would be most likely for ultrafine grain material where the diffusion distances are small or for any conditions which restrict the required atomic mobility at boundaries. If a threshold chemical potential is required to create or annihilate point defects, the creep would show Bingham behavior. However, if the annihilation and creation of defects involves climb of boundary dislocations in the plane of the boundary, the motion of these dislocations may be stress dependent as if limited by a viscous drag. By accounting for the stress dependence of dislocation density, a relation for strain rate of the form:[23]

$$\dot{\epsilon} = \frac{\alpha \sigma^2 b M}{\mu d} \qquad (5)$$

can be obtained where α is a numerical constant; b, the appropriate Burgers

vector of the boundary dislocation; M, the dislocation mobility; μ, the shear modulus; and d, the grain size. This predicts, as expected, that at fine grain sizes and low stresses, the interface reaction would be limiting, whereas under most conditions the creep rate would be given by the usual diffusional creep relation:[24]

$$\dot{\epsilon} = \frac{14\sigma\Omega D_\ell}{kTd^2}\left[1 + \frac{\pi\delta D_b}{d D_\ell}\right] \qquad (6)$$

where Ω is the ionic volume for the limiting species; D_ℓ, the lattice diffusivity; and δD_b, the grain boundary width diffusivity product.

Several characteristics of the deformation can be explained reasonably well assuming a diffusional creep model in which the interface reaction becomes important at grain sizes below about 5 μ and at lower stresses. The transition in the C126C material is of the proper form for sequential combination of eqns. (5) and (6). Using this assumption, the required diffusivities can be calculated from the stress-strain data using eqn. (6); under this assumption, the data should be taken from the high stress parts of the curves where the behavior is approaching m = 1. A stress of 20 Ksi was used which gives high m values for the C126C data, and allows use of the high purity 1 μ data and the 15 μ data without extrapolation.

The results* are shown in Figures 20 and 21 which show D_ℓ and δD_b, respectively. The individual data points shown on each graph were calculated assuming the strain rate to be entirely a result of either lattice or boundary diffusion, respectively. A single line does not fit all of the data points for either the boundary or lattice assumption, but a closer fit results for the boundary diffusion assumption. The lines shown were obtained assuming a possible contribution along both diffusion paths and then finding straight line plots of D_ℓ and δD_b to give the best total fit to the strain rate data using eqn. (6). An indication of the quality of the fit can be seen from the "+"s in Figure 21, which were obtained by calculating $\dot{\epsilon}$ from the D_ℓ line, subtracting from the experimental strain rate, and then calculating the resultant required δD_b. The C42 data points give the poorest fit, as anticipated since the expected increase in strain rate sensitivity was not indicated at the highest stresses tested (Figure 2), and so extrapolation to 20 Ksi may over estimate the actual strain rate. Since this material exhibited more cavitation at the higher stresses than the others, it is possible that this problem obscurred the expected increase in rate sensitivity. This slightly increases the activation energy of the δD_b line which would be obtained if only the 1 μ and 15 μ materials were considered.

These curves suggest that boundary diffusion is predominant for the fine grain materials at the low temperatures. For the 15 μ material, lattice diffusion would appear to be more important, but boundary diffusion appears to make an appreciable contribution especially at the lowest temperature. Comparison with the self-diffusion data[25,26] indicates much better agreement with the cation lattice diffusivity than with the anion diffusivity. However, the line is nearly a factor of 10 higher than the measured cation diffusivity and has a somewhat higher activation energy. The calculated boundary diffusivity is in the same range with other available calculated data from creep[27],

*A value of $\Omega = 2.12 \times 10^{-23}$ cm^3 was used which properly accounts for ambipolar effects on the assumption of cation diffusion as the limiting species.

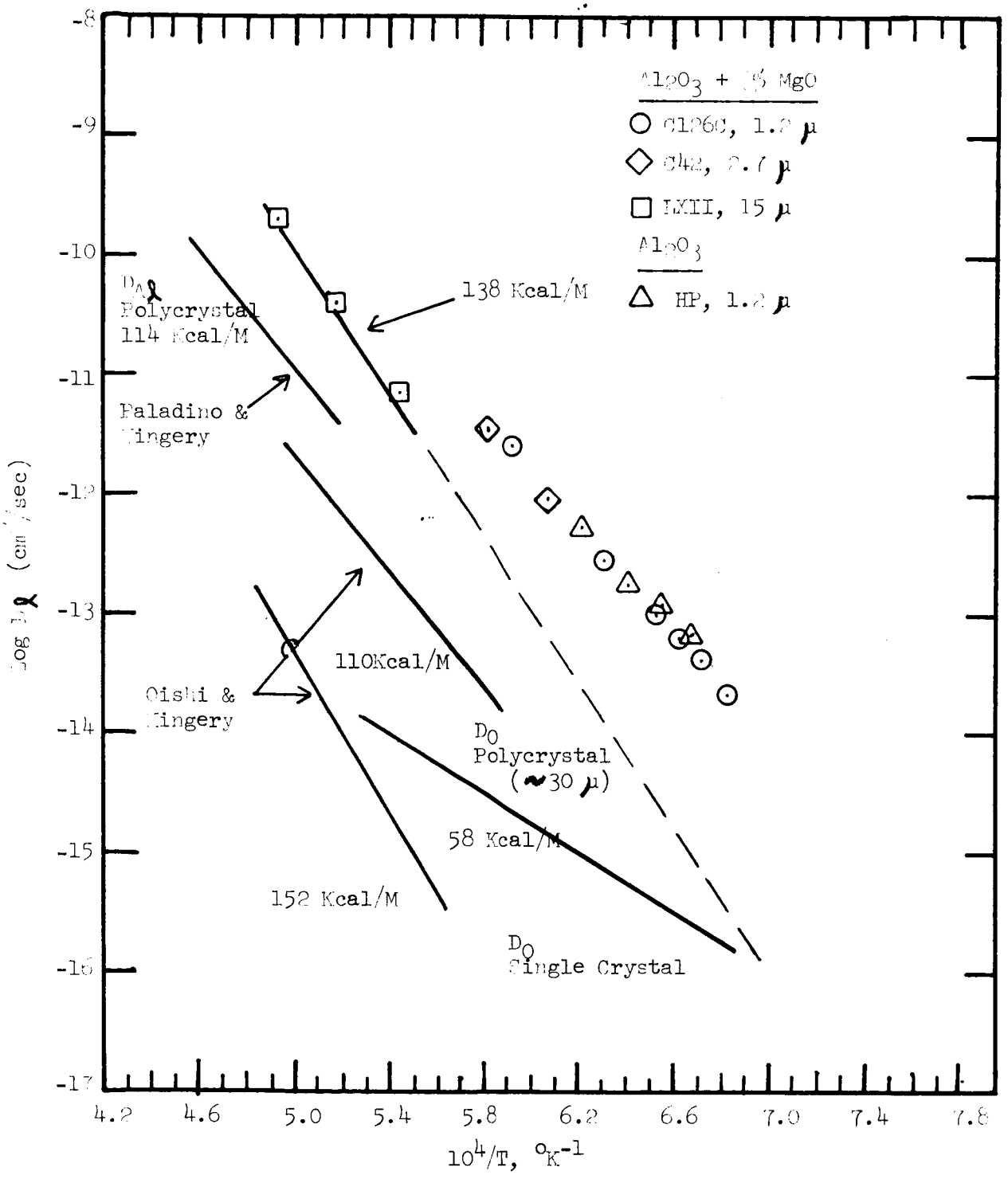

Figure 20. Apparent Lattice Diffusivity Calculated from the Diffusional Creep Relation. The individual data points are calculated assuming creep is entirely accounted for by lattice diffusion; the line is a fit to equation (6) assuming both lattice and boundary diffusion contribute.

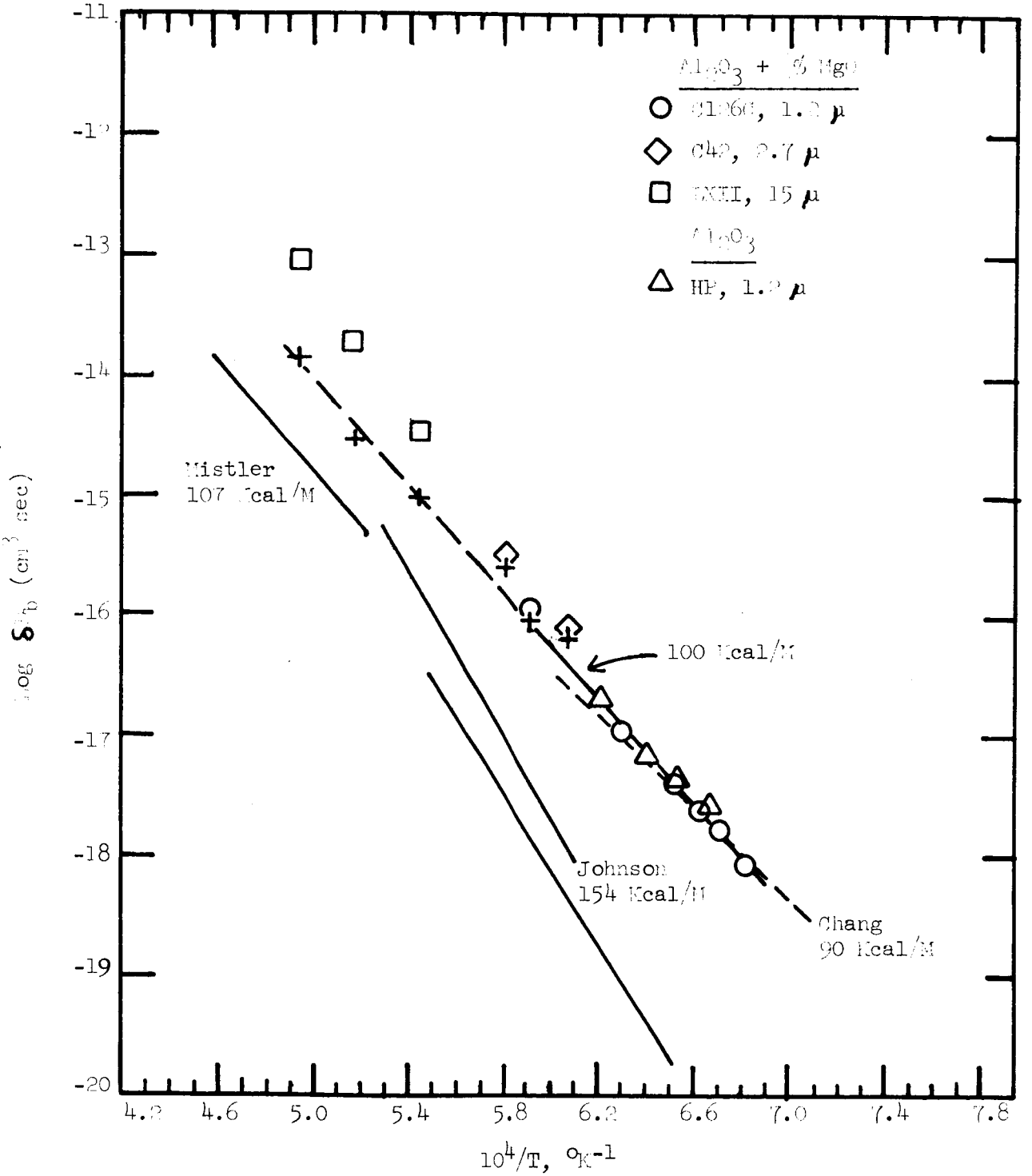

Figure 21. Apparent Boundary Width-Diffusivity Product Calculated from the Diffusional Creep Relation. The individual data points are calculated assuming the creep is entirely accounted for by boundary diffusion; the line is a fit to equation (6) assuming both lattice and boundary diffusion contribute. The points plotted as "+" were obtained by subtracting the calculated lattice contribution from the experimental strain rates; these points are omitted at low temperatures where the difference is less than 5%.

sintering[28], and grain growth studies.[29] This interpretation suggests that the aluminum ion is the slower diffusing species for all conditions tested. This interpretation requires, as has been suggested earlier[30], that the oxygen diffusion occurs exclusively via the boundaries and is faster than either aluminum ion, lattice, or boundary diffusion under all conditions of grain size and temperature investigated in this study. The higher value of the apparent diffusivity may reflect an increase in the cation lattice diffusion coefficient because of the MgO, as has been suggested by others for diavalent additives to Al_2O_3[31]; this would suggest that the cation diffusion is enhanced by an increased cation interstitial content. The higher activation energy may then reflect a contribution from Mg solubility, since the Mg content is above the solubility limit for all conditions. The similarity in behavior of the C126C and high purity material would seem to indicate little affect of MgO on the cation boundary diffusivity; however, the boundary diffusivity may be controlled by other impurities common to both materials.

An alternative explanation for the high diffusivities may be that the deformation involves more inhomogeneous strain from grain boundary sliding than is accounted for in the classical diffusional creep models. Recently, Ashby and Verall[23] have considered the possibility of grain boundary sliding with significant relative movement of grains, resulting in grains switching their neighbors, but with the necessary grain shape change accommodated by diffusion. The model predicts a stress-strain rate relation remarkably similar to the classical relation given in eqn. (6), but with the strain rate about a factor of seven higher than predicted by the classical model. This would lower the calculated lattice diffusivities into the range of measured cation diffusion data, and would be consistent with the microstructural observations which suggest significant boundary sliding. It may also offer a partial explanation for the fact that the various studies[3,13,19,32] of diffusional creep in Al_2O_3 result in a range of calculated diffusivities from near the measured cation diffusion data to about an order magnitude higher. Unfortunately, the conditions under which the two models may apply are not yet entirely clear except that it is suggested[23] that the inhomogeneous sliding behavior would become prevelant at higher strains.

An alternative explanation for diffusional creep behavior with mixed contributions from lattice and boundary diffusion would be to postulate that the coarser grained materials are limited by oxygen boundary diffusion and the finer materials by cation lattice diffusion with no contribution from boundary cation diffusion. An attempt to fit the data in Figures 20 and 21 to this model does not give as good a fit as does the cation boundary hypothesis; the projected lattice diffusivity would be about another factor of three higher at the high temperatures, but with a much lower activation energy. Further, the oxygen boundary diffusivity would have an activation energy of 130-140 Kcal/mol which seems too high. This hypothesis is also inconsistent with earlier studies[16,19] in which the grain size dependence was closer to G^{-2} for grain sizes of 5 to 30 u. As a result, the hypothesis of boundary enhanced cation diffusion at fine grain sizes with the indication that oxygen diffusion becomes limiting at grain sizes coarser than those measured here seems more reasonable.

This model explains the non-Newtonian behavior of the fine grain material as interface control. It would not be surprising then for the activation energy in this region to be different than that for the diffusion controlled

region as suggested by the C126C data. This activation energy would be characteristic of the non-conservative motion of boundary dislocations. Both boundary sliding and point defect emission and annihilation are currently considered to occur by motion of dislocations in the boundary[33,34] Although a simple model for boundary viscosity[33] suggests that the sliding, per se, should not be limiting, the understanding of these phenomena, especially in ceramics, is not yet sufficiently good to allow quantitative mechanistic analysis of the non-Newtonian regions. The strain rate dependence of $m = 0.5$ for the C126C material at low rates is consistent with the predictions of eqn. (5); however, direct comparison of the grain size dependence between the 1 μ and 3 μ materials in the non-Newtonian region gives $\dot{\varepsilon} \propto G^{-2.9}$ which is not consistent with the prediction of eqn. (5).

The major observation which the model of cation limited diffusional creep with interface control at fine grain sizes does not explain is the development of crystallographic texture and the importance of slip. The classical diffusional creep model predicts uniform strain of each grain and little, if any, change in texture. The inhomogeneous sliding model predicts significant rotation of individual grains which would randomize any initial texture. Further, observations on deformed superplastic alloys, generally considered to involve significant grain boundary sliding, have shown little textural development[35] and even randomization of an initial texture.[36] The observed formation of texture, even at low strain rates in the non-Newtonian regions, indicates that there is some slip occurring in the deformation of fine grained Al_2O_3; the low dislocation densities observed in transmission electron microscopy[3] indicate that the boundaries act as sources and sinks for dislocations and that few are trapped within grains. The significant difference in ease of activation of basal and non-basal slip systems, makes texture a probable result if there is a slip contribution.

One possible explanation is that slip occurs on any grains which are suitably oriented, especially where it can provide relief of stress concentrations from boundary sliding. If most of the slip is restricted to basal systems, then diffusion creep would have to provide shape change as an alternative to non-basal slip to satisfy the von Mises condition. In this case, the kinetics may still be limited by the presumably slower diffusional creep. If the strain contribution from slip changes slowly with stress and grain size, it would result in only a minor effect on the observed stress-strain rate-grain size dependences, except perhaps to increase the strain rate by nearly a constant factor over that predicted by the diffusional creep equation. This situation would explain the development of texture, but leave the above arguments concerning cation controlled diffusional creep in tact.

An alternative view is to suppose that the non-Newtonian behavior at fine grain sizes is a result of an increasing contribution of slip with increasing stress. Then at very low stresses, deformation would be purely diffusional, but as stress is increased, basal slip becomes possible in some grains with the number of grains in which it occurs increasing with stress giving a range of non-Newtonian behavior. The return to Newtonian behavior at high stress would result from the need for diffusional creep to satisfy the von Mises condition in the absence of significant non-basal slip. Since the significant regions of non-Newtonian behavior are not seen for the coarser

grained materials it would be assumed that the slip contribution does not become significant presumably because of the greater chance of intragranular dislocation interactions which would prevent easy escape to the boundaries. If this occurs, then strain rate dependence greater than $\dot{\epsilon} \propto G^{-2}$ would be in part a result of the increased contribution of slip at fine grain sizes and so separation of the lattice and boundary diffusion contributions would be more approximate. This alternative seems less plausible, however, since high temperature forgings[8,9] of coarser grained materials have shown significant development of texture and also recrystallization which indicates high internal strains from dislocation interactions.

Currently, there is still insufficient data to indicate the exact role of slip and the mechanisms of texture development. Further quantitative determinations of the rate of textural development over a range of stresses and grain sizes would be helpful in resolving this problem. Whatever the exact role of slip, it is likely that the sliding boundaries are important in dislocation generation, and that it will be most important in relieving the high local stress concentrations caused by boundary sliding. However, the similarity in the creep kinetics with the diffusion creep models indicates that diffusion also plays an important part in the accommodation process. From a practical consideration, further resolution of the current uncertainties is important in order to know whether the predictions of the diffusional creep model provide an upper or a lower bound to the deformation behavior of fine grained Al_2O_3.

The appearance and growth of cavities during deformation is not unexpected where appreciable grain boundary sliding occurs. Cavities will form where the stress concentrations are too high to be relieved by diffusion or slip and may continue to grow by point defect diffusion. However, the return to Newtonian behavior at high stresses for the 1 μ material and the fact that there may be worse cavitation in coarser materials which have higher rate sensitivities indicates that the non-Newtonian behavior in Al_2O_3 or other ceramics cannot be attributed only to cavitation. Further, the fine grained materials can be deformed to high strains under appropriate conditions without loss of density indicating that cavitation is only a possible result, but not a necessary consequence of grain boundary sliding. Of course, under conditions where there is serious cavitation, it may cause lower flow stresses and apparent rate sensitivities than would otherwise be observed. The higher fracture strengths of higher purity materials under conditions where plastic flow is occurring may result in part from a reduction of the scattered defects which influence fracture, but have little influence on the general deformation behavior; in addition, lower rates of cavitation may also result from stronger boundaries or possibly from higher mobility of grain boundaries allowing reduction of high stress concentrations.

IV. SUMMARY AND CONCLUSIONS

1. Studies of the high temperature deformation behavior of polycrystalline Al_2O_3 + $\frac{1}{4}$% MgO with grain sizes from 1-15 u were accomplished using constant rate flexure tests. Tests of a 1 μ material between 1192 - 1418°C revealed an apparent transition in behavior, characterized by a strain rate sensitivity of 0.5 at low strain rates and a shift to rate sensitivities approaching unity at high stresses. Comparison with available data for a higher purity undoped grade of Al_2O_3 revealed essentially similar behavior with no effect of the MgO on deformation behavior in the high rate sensitivity range where comparative data exist. Further, comparative tests on 1 u and 15 μ specimens revealed no significant effect of atmosphere between air and argon on the strain rate. Finally, an extended air anneal to remove possible carbonaceous or other gaseous impurities remaining from hot pressing, had no effect on flow stresses.

2. Determinations of crystallographic texture in compression tested samples of 1 μ material confirmed that a preferred orientation, with the c-axis parallel to the stress axes, develops in specimens deformed at temperatures as low as 1315°C at low stresses. This is taken as an indication of a contribution of dislocation slip to the deformation.

3. The form of the transition indicates a shift in control between two dependent deformation mechanisms. Comparison of the stress-strain rate-grain size dependencies in the high rate sensitivity range indicate that diffusional creep (diffusion accommodated grain boundary sliding) is one of the contributing deformation mechanisms. Calculated diffusion coefficients indicated that the process is controlled by cation boundary diffusion for the fine grain material especially at low temperatures. At higher temperatures and for the coarser grain sizes, cation lattice diffusion makes an increasing contribution. The calculated diffusivities are higher than the measured self-diffusivities and possible contributions of doping enhancement of diffusion, increased deformation from inhomogeneous boundary sliding, and slip contributions are discussed. The possible controlling mechanisms in the low rate sensitivity region including interface control resulting from imperfect point defect sources and sinks and slip contributions are discussed.

4. Additional attempts to deep draw hemispheres from blanks of Al_2O_3 were hindered by early cracking, apparently providing an indication of the need for good load and strain rate control in forging ceramics.

REFERENCES

1. R.M. Cannon and W.H. Rhodes, "Deformation Processes in Forging Ceramics," Summary Report, Contract NASW-1914 (June 1969 - August 1970).

2. a. W.H. Rhodes and R.M. Cannon, "Microstructural Studies of Refractory Polycrystalline Oxides," Summary Report, Contract N00019-70-C-0171, (April 1970 - February 1971).

   b. W.H. Rhodes and R.M. Cannon, "Microstructure Studies of Refractory Polycrystalline Oxides," Summary Report, Contract N00019-69-C-0198, (25 June 1969 - 24 December 1969).

3. A.H. Heuer, R.M. Cannon, N.J. Tighe, "Plastic Deformation in Fine-Grained Ceramics," in ULTRA-FINE GRAINED CERAMICS, ed. J.J. Burke, N.L. Reed, R. Weiss, Syracuse University Press (1970).

4. D.L. Holt and W.A. Backofen, Trans. ASM, 59, 755 (1966).

5. H.E. Cline and T.H. Alden, Trans. AIME, 239, 710 (1967).

6. W.A. Backofen, G.S. Murty and S.W. Zehr, Trans. AIME, 242, 329 (1968).

7. R.C. Bradt and J.H. Hoke, "Ceramic Research on Transformational Super-Plasticity and the Electron Microscopy of Ferroelectric Domain Boundaries," Progress Report, Contract AT(11-1)-3420, Pennsylvania State University (March 1, 1972).

8. A.H. Heuer, W.H. Rhodes, D.J. Sellers, and T. Vasilos, "Microstructure Studies of Polycrystalline Refractory Oxides," Avco Corp., Summary Report, Contract NOw-66-0506-(d) (1967).

9. A.H. Heuer, D.J. Sellers, and W.H. Rhodes, J. Am. Ceram. Soc., 52, 468 (1969).

10. R.M. Haag, "Magnetic-Crystallographic Orientation Produced in Ferrites by Hot-Working," Avco Corp., Contract N00014-68-C-0364, Annual Reports (March 1969 and March 1970).

11. W.H. Rhodes, P.F. Jahn, and P.L. Burnett, "Microstructural Studies of Polycrystalline Oxides," Summary Report, Contract N00014-68-C-0108 (25 May 1968 - June 24, 1969).

12. L.J. Broutman, S.M. Krishnakumar and P.K. Mullick, J. Am. Ceram. Soc., 53, 649 (1970).

13. R.M. Spriggs, J.B. Mitchell, and T. Vasilos, J. Am. Ceram. Soc., 47, 323 (1964).

14. W.H. Rhodes, D.J. Sellers, R.M. Cannon, A.H. Heuer, W.R. Mitchell, and P. Burnett, "Microstructure Studies in Polycrystalline Refractory Oxides," Avco Summary Report, Contract N000-19-67-C-0336 (1968).

REFERENCES cont.

15. R.C. Folweiler, J. Appl. Phys., 32, 773 (1961).

16. M.L. Kronberg, J. Am. Ceram. Soc., 45, 274 (1962).

17. H. Conrad, G. Stone, and K. Janowski, Trans. AIME, 233, 89 (1965).

18. J.B. Wachtman, Jr. and L.H. Maxwell, J. Am. Ceram. Soc., 40, 377 (1957).

19. S.I. Warshaw and F.N. Norton, J. Am. Ceram. Soc., 45, 479 (1962).

20. M.F. Ashby, Scripta. Met., 3, 837 (1969).

21. G.W. Greenwood, Scripta. Met., 4, 171 (1970).

22. B. Burton, Mat. Sci. & Eng., 10, 9 (1972).

23. M.F. Ashby and R.A. Verrall, "Diffusion-Accommodated Flow and Superplasticity," Harvard Technical Report No. 6 (1972 June).

24. R. Raj and M.F. Ashby, Met. Trans., 2, 1113 (1971).

25. Y. Oishi and W.D. Kingery, J. Chem. Phys., 33, 480 (1960).

26. A.E. Paladino and W.D. Kingery, J. Chem. Phys., 37, 957 (1962).

27. R. Chang, "Diffusion-Controlled Deformation and Shape Changes in Nonfissionable Ceramics," in Proceedings of the Conference on Nuclear Application of Nonfissionable Ceramics, ed. A. Boltax and J.H. Handwerk, Am. Nuclear Soc., Hinsdale, Illinois (1966).

28. D.L. Johnson and L. Berring, "Grain Boundary Diffusion in the Sintering of Oxides," in SINTERING AND RELATED PHENOMENA, eds. G.C. Kuczynski, N.A. Hauton, and C.G. Gibbon, Gordon & Breach, New York (1967).

29. R.E. Mistler, "Grain Boundary Diffusion and Boundary Migration Kinetics in Aluminum Oxide, Sodium Chloride and Silver," Sc.D. Thesis, M.I.T. (1967).

30. A.E. Paladino and R.L. Coble, J. Am. Ceram. Soc., 46, 133 (1963).

31. G.W. Hollenberg and R.S. Gordon, "The Effect of Oxygen Partial Pressure on the Creep of Polycrystalline Al_2O_3 Doped with Transition Metal Impurities (Cr, Fe, Ti)," presented at the Basic Science Fall Meeting, Am. Ceram. Soc. (1971).

32. R.L. Coble and Y.H. Guerard, J. Am. Ceram. Soc., 46, 353 (1963).

33. M.F. Ashby, "Boundary Defects and Atomistic Aspects of Boundary Sliding and Diffusional Creep," in GRAIN BOUNDARIES AND INTERFACES, eds. P. Chaudhari and J.W. Matthews, North-Holland, Amsterdam (1972).

REFERENCES concluded

34. R.N. Stevens, "Grain Boundary Sliding and Diffusional Creep," in GRAIN BOUNDARIES AND INTERFACES, eds. P.Chaudhari and J.W. Matthews, North-Holland, Amsterdam (1972).

35. D. Lee, J. Inst. of Metals, 99, 66 (1971).

36. C.P. Cutler and J.W. Edington, Met. Sci. J., 5, 201 (1971).

APPENDIX

An analysis was presented previously[1] in which the effects on the bending moment of horizontal loads at the support points were treated for plastic bending. For a flat specimen in four point loading, the bending moment in the gauge section is given by:

$$M_S = \frac{Pa}{2} \tag{A1}$$

where P is the total applied load and a is the moment arm. For plastic bending, the deflections can be significant even for relatively short beams and the horizontal load components must be considered. In this case, the correction to the bending moment in the gauge section is given by:

$$\frac{M}{M_S} = 1 + \frac{1}{a}\left(\frac{\sin\psi_1 - \mu\cos\psi_1}{\cos\psi_1 + \mu\sin\psi_1}\right)\left(y - \frac{h}{2\cos\psi_1}\right) - \frac{1}{a}\left(\frac{\sin\psi_2 + \mu\cos\psi_2}{\cos\psi_2 - \mu\sin\psi_2}\right)\left(y - y_2 + \frac{h}{2\cos\psi_2}\right) \tag{A2}$$

$$(0 \le x < L/2 - a)$$

where the relevant geometry is defined in Figure A1 and μ is the coefficient of friction between the load supports and the specimen. A similar correction exists for the moment in the moment arm regions:

$$\frac{M}{M_S} = 1 + \frac{1}{L/2 - a}\left(\frac{\sin\psi_1 - \mu\cos\psi_1}{\cos\psi_1 + \mu\sin\psi_1}\right)\left(y - \frac{h}{2\cos\psi_1}\right) \tag{A3}$$

$$(L/2 - a < x \le L/2)$$

where this region:

$$M_S = \frac{Pa}{2}\left(L/2 - x\right) \tag{A4}$$

Applying these corrections for plastic bending requires determination of y, ψ_1, and ψ_2, for all X, since they will be affected by the constituitive relation of the material and by μ. Determination of these quantities continuously during high temperature tests would be difficult and was not attempted during this work. Further, uncertainty about the value of μ, also makes quantitative correction difficult since it significantly affects the results. However, for probable values of the coefficient of friction, this effect could account for some of the non-linearity in the $\sigma - \dot{\epsilon}$ curves of the C126C material and should be qualitatively considered.

The difficulty arises because the strain required to achieve steady-state in the bend tests increases with the strain rate and stress and so a systematic error can be introduced in the $\sigma - \dot{\epsilon}$ plots in which the greatest error from large curvature occurs at the highest rates. To indicate the magnitude of the effect a series of M/M_S curves versus outer fiber strain were calculated for several values of μ. If u is independent of load, the correction is simply a function of the specimen geometry. An approximate set of y, ψ_1, and ψ_2 values were calculated from the linear elastic deflection relation; this gives a reasonable approximation to specimen geometry for highly rate sensitive materials. These values were then used to calculate the M/M_S ratios shown in Figure A2, which are for the center of the gauge length. The effect of the linear elastic geometrical approximation can be seen from the individual points at 4.5% strain, which were calculated on the

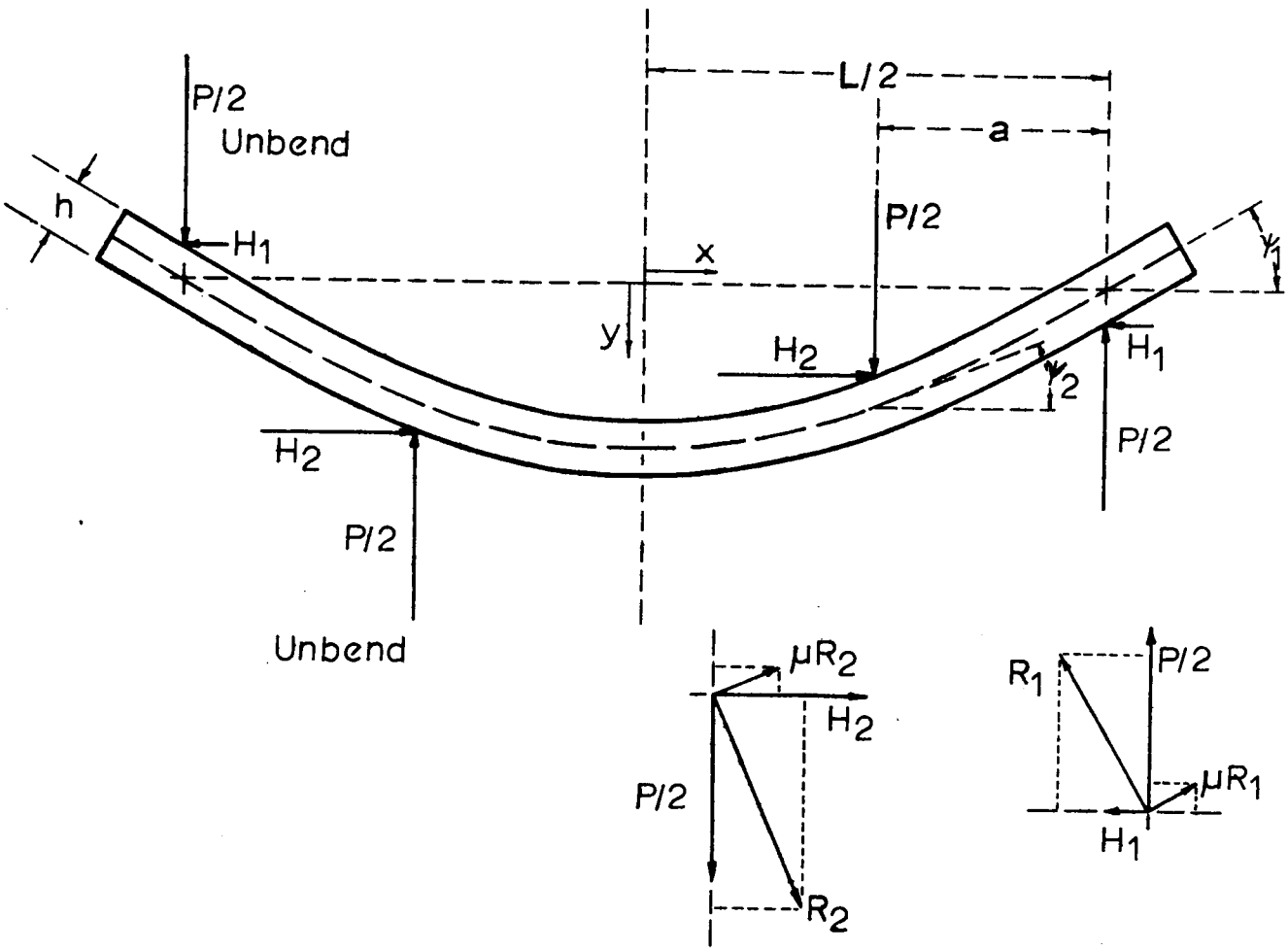

Figure A1. Schematic of Curved Bend Bar Showing Relevant Geometry; Resolution of the forces at the inner and outer supports is also shown.

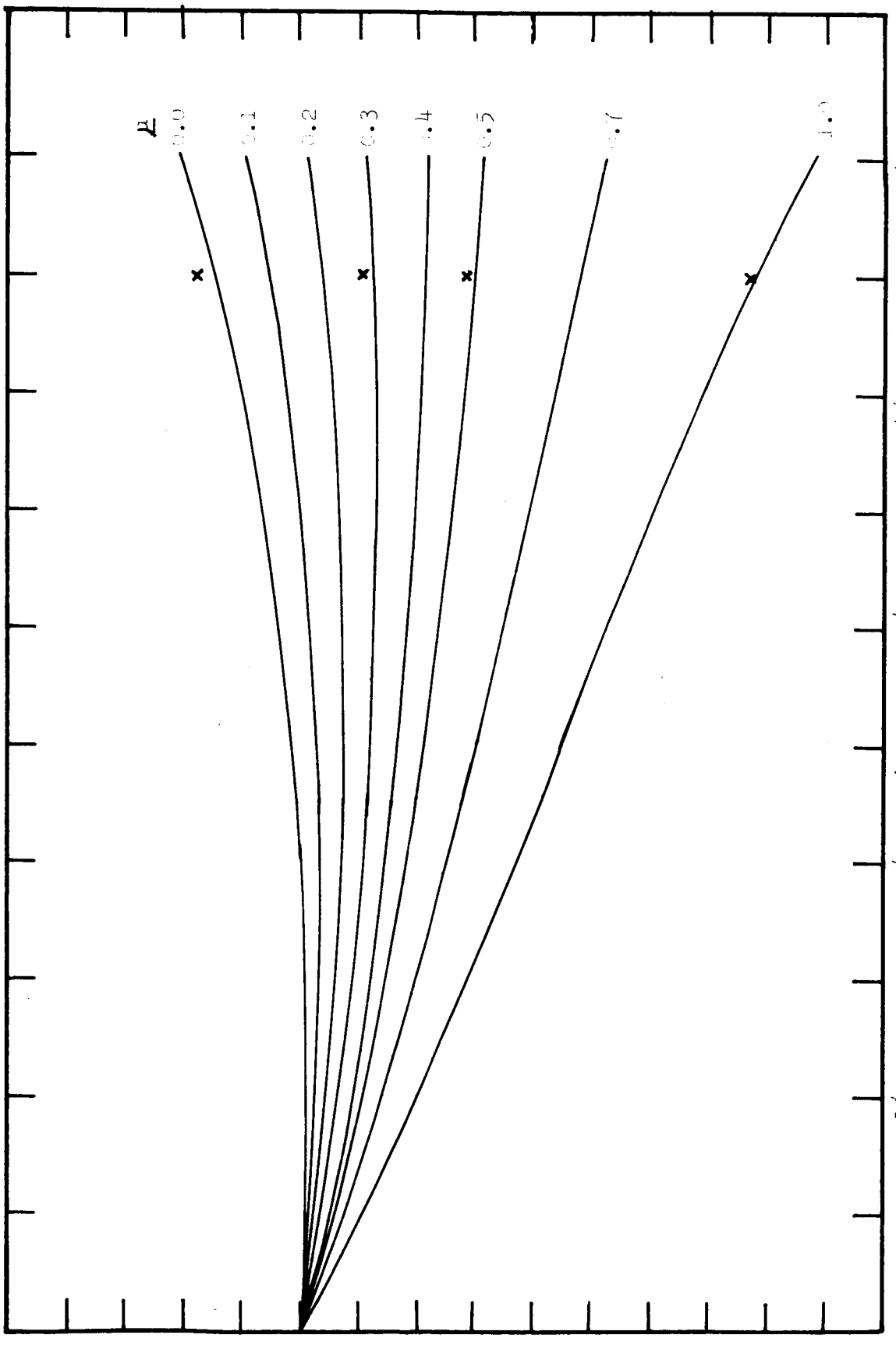

Figure -2. Moment Correction Ratio, M/Ms, Calculated for the Parameter of the Bauschinger Effect and the Nonlinear Elastic Curvature Relation with the Coefficient of Friction, μ, as a Parameter.

basis of the measured final geometry of a C126C bend specimen[1]; especially at intermediate values of μ, there is little error. The errors arise since the bending in the moment arm is less for non-Newtonian, i.e., $m \neq 1$, plastic bending, and because the correction for the horizontal loads is not uniform along the bar. This can also cause the moment in the gauge section to become non-uniform. For comparison, the moment, calculated on the same set of assumptions, at the end of the gauge section is shown in Figure A3. For small μ, the moment is nearly uniform across the gauge length, but for larger values of μ, the moment will be lower in the center than near the inner load supports.

For the tests in argon, 0.005 inch tungsten foil spacers were generally used between the specimen and knife edges to reduce knife edge abrasion. For the air tests, platinum proved to be too soft and, therefore, no spacers were used between the specimen and the coarse grained Al_2O_3 knife edges. At the test temperatures, no significant contaminating films which would provide lower friction would be expected to remain and therefore very low values of μ would be unlikely. By considering the coefficients of friction reported for sapphire at low temperature and for the hcp metals (since Al_2O_3 is hexagonal and anisotropic), values of μ from 0.2 up to 0.7 would seem plausible. In anticipation of this problem, the total strains in the C126C tests were generally limited to about 3% or less.

If μ were as high as 0.7, then by the end of a test the stress values calculated from the simple moments could be too high by as much as 25%; if μ were only 0.2%, the error would be less than 10%. Comparison of the individual data points suggested that some of the scatter could be accounted for by horizontal load effects and further suggested some variation in μ occurs from test to test. For values of μ much in excess of 0.7, the net axial force becomes appreciable; this combined with the variation of moment within the gauge section, would cause the specimen to exhibit a significant deviation from uniform bending. Such behavior was not observed and so this seems a likely upper bound on μ.

Although it could be argued that the increase in rate sensitivity observed for the C126C material was entirely an artifact caused by the curvature effect on the moment, this seems unlikely for two reasons. First, unreasonably high values of μ would be necessary to account for the entire effect; secondly, tests on coarser grained materials, with m near unity, have been run to large strain values, over a comparable stress range, without appreciable changes in the apparent rate sensitivity.

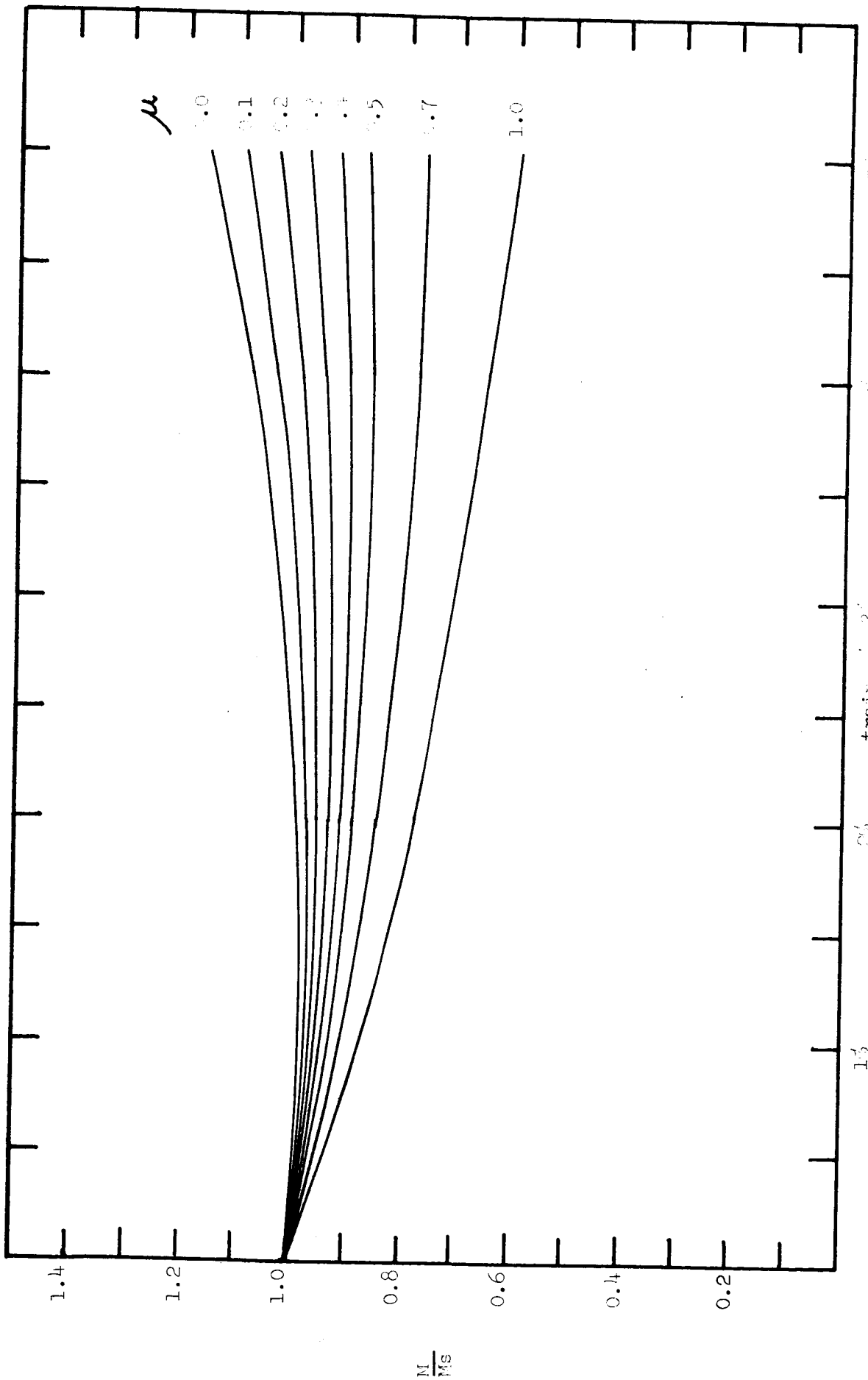

Figure A-3. Cone tip correction ratio, M/M_s, calculated for the end of the cone penetration in linear elastic curvature relation, ϕ, for the coefficient of friction, μ, parameter.